Published April 9, 2012

The Arp2/3 complex is required for lamellipodia extension and directional fibroblast cell migration

Praveen Suraneni,[1] Boris Rubinstein,[1] Jay R. Unruh,[1] Michael Durnin,[1] Dorit Hanein,[2] and Rong Li[1,3]

[1]Stowers Institute for Medical Research, Kansas City, MO 64110
[2]Bioinformatics and Systems Biology Program, Sanford-Burnham Medical Research Institute, La Jolla, CA 92037
[3]Department of Molecular and Integrative Physiology, University of Kansas Medical Center, Kansas City, KS 66160

The Arp2/3 complex nucleates the formation of the dendritic actin network at the leading edge of motile cells, but it is still unclear if the Arp2/3 complex plays a critical role in lamellipodia protrusion and cell motility. Here, we differentiated motile fibroblast cells from isogenic mouse embryonic stem cells with or without disruption of the ARPC3 gene, which encodes the p21 subunit of the Arp2/3 complex. ARPC3$^{-/-}$ fibroblasts were unable to extend lamellipodia but generated dynamic leading edges composed primarily of filopodia-like protrusions, with formin proteins (mDia1 and mDia2) concentrated near their tips. The speed of cell migration, as well as the rates of leading edge protrusion and retraction, were comparable between genotypes; however, ARPC3$^{-/-}$ cells exhibited a strong defect in persistent directional migration. This deficiency correlated with a lack of coordination of the protrusive activities at the leading edge of ARPC3$^{-/-}$ fibroblasts. These results provide insights into the Arp2/3 complex's critical role in lamellipodia extension and directional fibroblast migration.

Introduction

Fibroblasts are migratory cells of the connective tissue playing important roles in wound healing and mediating the formation and remodeling of epithelial tissues (Tomasek et al., 2002; Kalluri and Zeisberg, 2006). In vitro, cultured fibroblasts have been used as a model system for studying the signaling and mechanical processes of cell migration. A migrating fibroblast on a 2D matrix exhibits the stereotypical polarized morphology with an often fan-shaped front called the lamella and a tapered tail end (Abercrombie and Heaysman, 1954; Abercrombie et al., 1971). At the leading edge of the lamella, two types of protrusive structures are frequently observed, the ruffling veil-like lamellipodia and the thin, spike-like filopodia. Ultrastructural data showed that lamellipodia are composed of orthogonal arrays of actin filaments with branched actin filaments near the leading edge plasma membrane, whereas filopodia contain parallel bundles of actin filaments (Chhabra and Higgs, 2007). Elongation at the barbed ends of actin in lamellipodia and filopodia is thought to produce the protrusive force for leading edge advancement (Pollard and Borisy, 2003; Bugyi and Carlier, 2010). Protein factors regulating actin polymerization at the leading edge are thus key components of the molecular machinery driving cell motility.

The Arp2/3 complex is an evolutionarily conserved actin nucleation factor localized in the lamellipodia (Mullins et al., 1996; Welch et al., 1997; Pollard, 2007). The Arp2/3 complex is composed of seven stoichiometric subunits, including two actin-related proteins, Arp2 and Arp3, and five additional subunits, ARPC1–5 (Machesky et al., 1994; Welch et al., 1997; Winter et al., 1997; Bugyi and Carlier, 2010). Purified Arp2/3 complex does not (or poorly) stimulate actin nucleation, but in the presence of nucleation promoting factors, most importantly Wiskott-Aldrich Syndrome protein (WASP) family members, the Arp2/3 complex nucleates a new actin filament from the side of an existing filament (Machesky et al., 1997; Mullins et al., 1998; Rohatgi et al., 1999; Winter et al., 1999; Volkmann et al., 2001; Rouiller et al., 2008). The resulting actin structures are highly reminiscent of the branched actin network observed in lamellipodia. (Svitkina and Borisy, 1999; Yang and Svitkina, 2011). The Arp2/3 complex also nucleates branched actin network at the surface of the pathogenic bacteria, *Listeria monocytogenes*, as part of the actin comet tail propelling the bacterium's motility within host cell cytoplasm (Welch et al., 1998; Loisel et al., 1999; May et al., 1999; Yarar et al., 1999). These findings

Correspondence to Rong Li: rli@stowers.org

Abbreviations used in this paper: ES, embryonic stem; FLP, filopodia-like protrusions; iMEF, irradiated mouse embryonic fibroblast; LIF, leukemia inhibiting factor; MSD, mean square displacement.

Supplemental Material can be found at:
http://jcb.rupress.org/content/suppl/2012/04/05/jcb.201112113.DC1.html
Original image data can be found at:
http://jcb-dataviewer.rupress.org/jcb/browse/5362

The Rockefeller University Press $30.00
J. Cell Biol. Vol. 197 No. 2 239–251
www.jcb.org/cgi/doi/10.1083/jcb.201112113

Published April 9, 2012

led to the dendritic nucleation model for the generation and extension of the lamellipodial actin network by the Arp2/3 complex (Pollard and Borisy, 2003). In addition, debranching and bundling of the Arp2/3 complex–nucleated actin filaments is thought to be a major pathway for filopodia formation (Svitkina et al., 2003; K. Lee et al., 2010).

Although the dendritic nucleation model has been rigorously evaluated in several computational studies (Maly and Borisy, 2001; Schaus et al., 2007; Schaus and Borisy, 2008), experimental evidence demonstrating a critical role for Arp2/3 in the generation of protrusive actin structures and cell motility has been far from clear. Although some of the studies using RNAi against Arp2/3 components or dominant-negative constructs derived from WASP family proteins concluded that disrupting the Arp2/3 inhibited lamellipodia formation or morphology (Machesky and Insall, 1998; Bailly et al., 2001; Steffen et al., 2006), one study reported a lack of effect on lamellipodia extension or morphology even after knocking down complex subunits by over 90% in mouse embryonic fibroblasts (Di Nardo et al., 2005). However, given that the Arp2/3 complex nucleates actin at nanomolar concentrations (Higgs and Pollard, 1999), even a dramatic knockdown could still leave behind a level sufficient to fully or partially support Arp2/3-dependent functions. Importantly, none of the published studies analyzed in detail the impact of Arp2/3 complex inhibition on fibroblast cell motility.

The goal of this study is to genetically disrupt the Arp2/3 complex in order to determine its function in fibroblast cell motility. We derived mouse embryonic stem (ES) cell lines from isogenic ARPC3$^{-/-}$ and ARPC3$^{+/+}$ blastocysts. Differentiation of the ES cells into fibroblasts enabled us to perform detailed microscopy analyses comparing leading edge structures, dynamics, and motility behaviors between cells of these two genotypes in vitro. Our results show that in the absence of the Arp2/3 complex, fibroblasts are unable to form stereotypical lamellipodia or undergo sustained directional migration. The system developed in this study can be used for determining the role of the Arp2/3 complex in the motility of diverse cell types that can be differentiated from ES cells.

Results and discussion

Generation of ARPC3$^{-/-}$ and ARPC3$^{+/+}$ ES cells and fibroblast differentiation

Our initial choice of targeting the ARPC3 subunit of the Arp2/3 complex was due to the availability of a mouse ES cell line (Bay Genomics) bearing heterozygous gene-trap disruption of the single gene encoding ARPC3, the p21 subunit of the Arp2/3 complex. Biochemical analysis of the yeast and human Arp2/3 complexes previously showed that although a partial complex can exist in the absence of p21, the nucleation-promoting factor–stimulated actin nucleation is severely disrupted (Gournier et al., 2001; Kreishman-Deitrick et al., 2003). The gene-trap cassette used by Bay Genomics contained a promoterless reporter/selectable marker fusion gene (βgeo) followed by a strong transcriptional termination sequence (Wiles et al., 2000; Stanford et al., 2001). In the ARPC3 gene-trap ES cell line (XG476), the gene trap was inserted in the second intron of the ARPC3 gene, leading to truncation of ARPC3 after exon 2 (at amino acid 36) by βgeo (Fig. S1 A), as confirmed by 5′ RACE PCR analysis. XG476 ES cells were used to generate ARPC3$^{+/-}$ mice in the C57BL/6J genetic background (see Materials and methods). ARPC3$^{+/-}$ adult mice appeared normal and fertile; however, no live ARPC3$^{-/-}$ homozygous newborns were observed. Further genotyping of embryos from embryonic day E3.5, E8.5, and E10.5 indicated that ARPC3$^{-/-}$ causes embryonic lethality as early as E3.5, the blastocyst stage (Fig. S1 B). A similar pre-implantation embryonic lethality was also reported in a study in which *ARPC3* was disrupted by transposon insertion (Yae et al., 2006).

Although unable to undergo implantation and further development, the ARPC3$^{-/-}$ blastocysts appeared to contain well-formed inner cell mass cells (Fig. S1 B), suggesting the possibility of using these blastocysts to derive ES cells. To this end, blastocysts were collected after mating of ARPC3$^{+/-}$ parents and cultured individually on irradiated mouse embryonic fibroblast (iMEF) feeder layers in ES cell medium containing leukemia inhibiting factor (LIF). The genotype of the ES cells derived from each blastocyst was determined retrospectively by PCR assays of the genomic DNA (Fig. S2 A). The pluripotency of the resulting ARPC3$^{+/+}$, ARPC3$^{+/-}$, and ARPC3$^{-/-}$ ES cell clones was assessed by using standard methods including anti-Oct4 immunofluorescence staining and the alkaline phosphatase assay (Fig. S2 B; Thomson et al., 1998; Singh et al., 2008; J. Lee et al., 2010; Griffith et al., 2011).

We used a previously established protocol to differentiate ES cells into fibroblasts. In brief, ES cells were separated from the feeder cells and then cultured without LIF but in the presence of retinoic acid for 7 d (Smith, 1991). At the end of this culturing, the differentiated fibroblasts were separated from the remaining undifferentiated ES cells based on the ability of fibroblasts to rapidly readhere to fibronectin-coated substrate after trypsinization. The fibroblast identity of these differentiated cells was further confirmed by staining of a commonly used fibroblast marker, IB10 (Fig. S3 A; Pease et al., 1990; Rønnov-Jessen et al., 1992). PCR genotyping was performed on the differentiated fibroblasts to reconfirm their genetic identity. RT-PCR showed that although full-length ARPC3 mRNA was detected in the ARPC3$^{+/+}$ fibroblasts, no amplicon was observed in samples from ARPC3$^{-/-}$ fibroblasts (Fig. S2 C), confirming disruption of ARPC3 expression by the gene trap as expected. Immunofluorescence showed no ARPC3 staining in the mutant cells, whereas lamellipodia staining was observed in ARPC$^{+/+}$ cells (Fig. S3 B). Possibly as a result of the inability to form a full complex, immunoblotting showed that the protein level of Arp2 was dramatically reduced in the mutant compared with wild-type cells (Fig. S2 D).

ARPC3$^{-/-}$ fibroblast cells are defective in the formation of lamellipodia

Although the differentiated fibroblasts of both ARPC3$^{+/+}$ and ARPC3$^{-/-}$ genotypes showed the flat morphology with protrusive edges as expected, it was readily apparent that whereas wild-type fibroblasts had smooth lamellipodia-like edges and some spiky protrusions that morphologically resembled filopodia, the mutant cells displayed jagged edges exclusively with

Published April 9, 2012

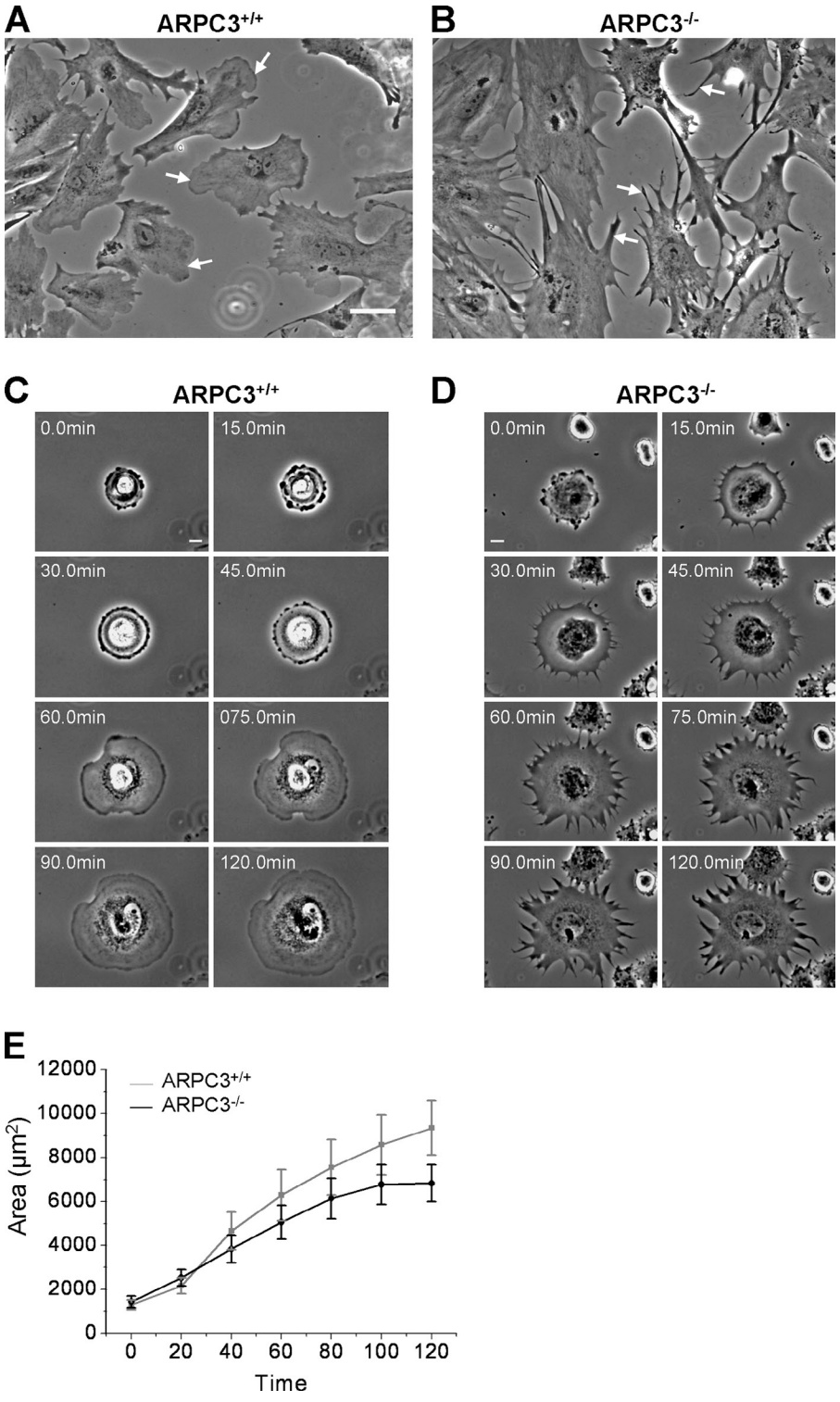

Figure 1. **ARPC3$^{-/-}$ fibroblast cells are deficient in lamellipodia formation.** (A and B) Representative phase-contrast images showing the morphology of ARPC3$^{+/+}$ (A) and ARPC3$^{-/-}$ (B) fibroblast cells after 7 d of differentiation. Arrows indicate lamellipodia (wild type) and FLPs (mutant). Bar, 50 µm. (C and D) Time-lapse montage showing spreading morphology of ARPC3$^{+/+}$ (C) and ARPC3$^{-/-}$ cells (D) on 5 mg/ml fibronectin-coated glass surface. Frame interval is 15 min. Bars, 15 µm. (E) Quantification of cell area from experiments as described in C and D. Plots show mean and standard error of the mean (SEM) from 13 (APRC3$^{+/+}$) and 11 (APRC3$^{-/-}$) spreading cell movies made in three different experiments.

the latter (Fig.1, A and B, arrows). Because the morphologies of the cells in each population were somewhat heterogeneous, depending on whether they were in contact with other cells or whether they were actively moving, we compared the morphology of protrusive cell edges in a spreading assay where the cells were expected to have a more uniform morphology. Cells were first detached from the substrate by trypsinization and then allowed to re-spread on fibronectin-coated coverslips, during which the morphology of the cells was recorded by time-lapse imaging. Fig. 1, C and D, show a montage of representative of ARPC3$^{+/+}$ and ARPC3$^{-/-}$ cells (also see Videos 1 and 2). All of the observed ARPC3$^{+/+}$ cells that spread (n = 10) did so through highly uniform lamellipodia extension positive for phalloidin and anti-Arp2 staining (Fig. 2 A). By contrast, none of the ARPC3$^{-/-}$ cells observed to spread (n = 10) showed veil-like edges, but instead spread through protrusions that contained

Published April 9, 2012

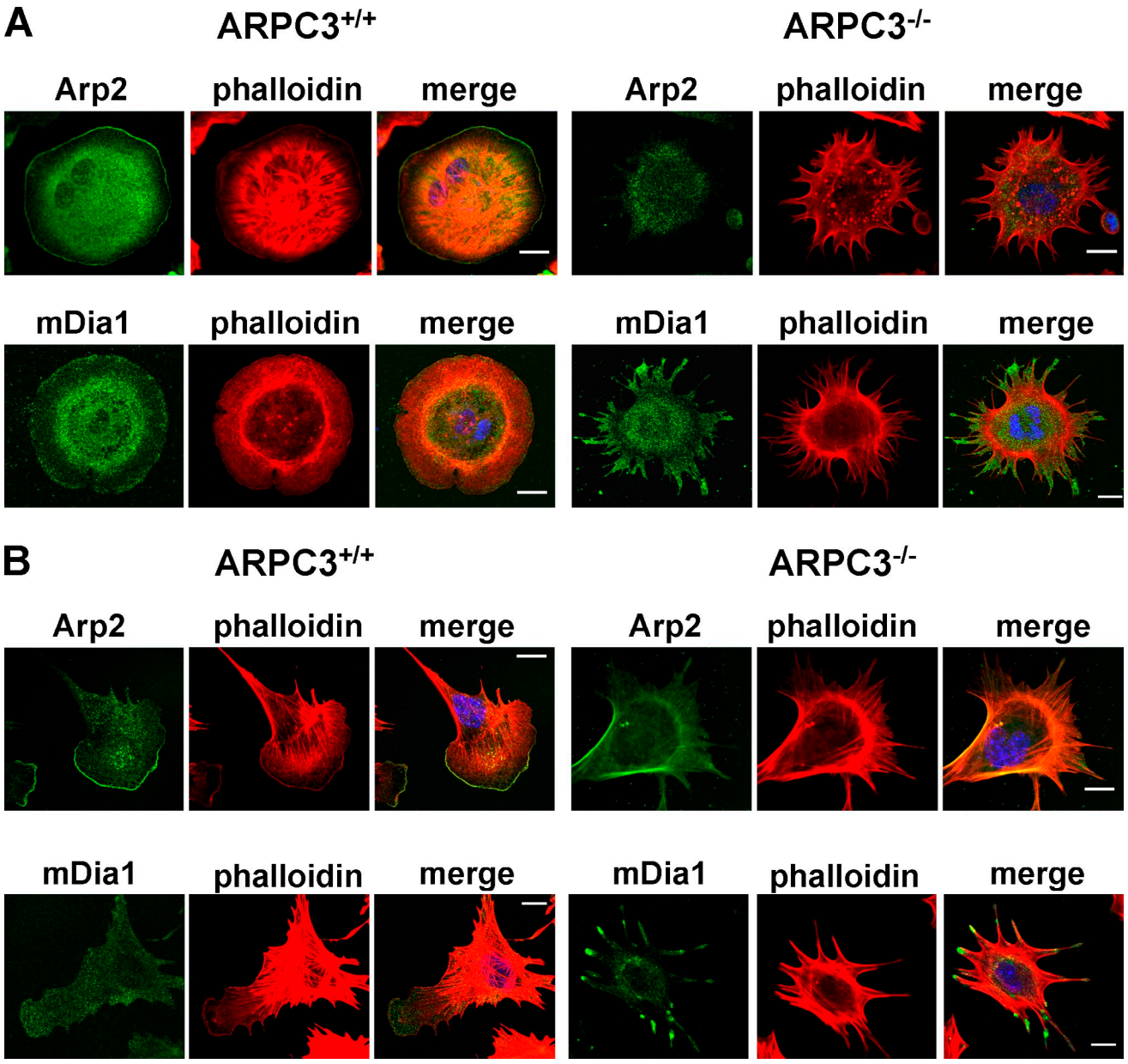

Figure 2. **Localization of Arp2 and mDia1 formin in ARPC3$^{+/+}$ and ARPC3$^{-/-}$ fibroblasts.** Spreading (A) or polarized (B) ARPC3$^{+/+}$ and ARPC3$^{-/-}$ cells were fixed and stained with AF546 phalloidin (red), the indicated antibodies (green), and DAPI (blue). Bars, 25 µm.

actin bundles (Fig. 2 A) and fascin (Fig. S3 B), an actin-bundling protein found in filopodia (Vignjevic et al., 2006; Zigeuner et al., 2006; Valkov et al., 2011). For simplicity, the spiky, fascin-containing protrusions in the ARPC3$^{-/-}$ fibroblasts are referred to hereafter as filopodia-like protrusions (FLPs). Interestingly, the mutant cells spread nearly as efficiently as the wild type (Fig.1E), although a slight deficiency is consistent with a previous study (Nicholson-Dykstra and Higgs, 2008).

Phalloidin staining of polarized ARPC3$^{+/+}$ and ARPC3$^{-/-}$ fibroblasts show that although the wild-type cells exhibit the typical actin organization with F-actin enriched at the lamellipodia leading edge and stress fibers extending into the lamella (Fig. 2 B), the leading edges of mutant cell are characterized by FLPs that contain actin bundles and fascin (Fig. 2 B and Fig. S3 C), followed by prominent transverse actin arcs (Fig. 2 B).

We next stained the cells with antibodies against the known actin-nucleating proteins in lamellipodia and filopodia. Staining with an anti-Arp2 antibody confirmed that although the Arp2/3 complex localizes to the actin-rich lamellipodia of spreading or polarized ARPC3$^{+/+}$ fibroblast cells, it is absent from the tip of the actin bundles in the FLPs in ARPC3$^{-/-}$ cells, and only diffuse cytoplasmic staining was observed (Fig. 2). As formins are potent actin nucleation factors previously implicated in filopodia formation (Peng et al., 2003; Higashida et al., 2004; Pellegrin and Mellor, 2005; Schirenbeck et al., 2005; Yang et al., 2007; Block et al., 2008; Harris et al., 2010), we stained the fibroblasts with antibodies against Diaphanous-related formins (DRF) mDia1 and mDia2. Although neither protein is prominently localized at the lamellipodia in ARPC3$^{+/+}$ fibroblasts, both DRFs were found to localized at the tips of the actin-rich

Published April 9, 2012

protrusions in ARPC3$^{-/-}$ fibroblasts (Fig. 2 and Fig. S3 C), suggesting that these protrusions might be formed through DRF-mediated actin assembly. Immunoblotting found that the level of mDia1 protein was not drastically different in the mutant compared with the wild type (Fig. S2 E).

ARPC3$^{-/-}$ fibroblasts are defective in wound healing in vitro due to a lack of sustained migration directionality

Wound healing is one of the main functions for fibroblasts and requires migration of these cells toward the epithelial wound (Diegelmann and Evans, 2004; Gurtner et al., 2008). We used an in vitro assay to assess the ability of ARPC3$^{-/-}$ cells to undergo wound healing. ARPC3$^{+/+}$ and ARPC3$^{-/-}$ fibroblasts were plated at the same densities to form a confluent monolayer before a wound of 300–400 µm was generated by using a culture insert (see Materials and methods). Wound closure was monitored by taking microscopy images at different time points after wound creation. ARPC3$^{+/+}$ cells took ∼30 h to complete wound closure, whereas ARPC3$^{-/-}$ cells showed a considerable delay in wound closure: even after 54 h, the wound reduced in size but was not completely closed (Fig. 3, A–C). We note that ARPC3$^{+/+}$ and ARPC3$^{-/-}$ fibroblasts are slowly dividing cells with doubling time ∼56 h and limited proliferative potential, and thus cell division was unlikely to contribute significantly to wound closure.

Time-lapse phase-contrast movies were made to observe the migration of ARPC3$^{+/+}$ and ARPC3$^{-/-}$ fibroblasts during wound healing. We focused on the behavior of cells at the edge of the wound moving into the open space. As shown in Video 3, ARPC3$^{+/+}$ cells moved toward the wound with leading edges exhibiting the expected lamellipodia morphology (also see Fig. 3 D). By contrast, ARPC3$^{-/-}$ cells migrated into the wound exclusively with FLP-rich leading edges (Video 4 and Fig. 3 D). To quantitatively compare the dynamics of the leading edge between wild-type and mutant cells we used a kymograph analysis to obtain parameters, including the rate of protrusion or retraction and duration of protrusion or retraction (Fig. 3, D and E). Surprisingly, this analysis found that ARPC3$^{-/-}$ fibroblasts display significantly faster leading edge protrusion and retraction rates than the corresponding rates of the lamellipodia in ARPC3$^{+/+}$ cells (Table S1). The durations of the protrusion or retraction phases in the mutant cells are also slightly but significantly longer than those in the wild type.

As it was non-obvious that the above parameters describing leading edge dynamics could account for the wound-healing defect observed for ARPC3$^{-/-}$ fibroblasts compared with ARPC3$^{+/+}$ fibroblasts, we went on to analyze whole-cell motility behaviors from long time-lapse movies by tracking the movement of individual ARPC3$^{+/+}$ or ARPC3$^{-/-}$ cells toward the wound area (Fig. 4, A and B; Videos 5 and 6). Care was taken to track only those cells moving independently into the wound area, as interaction with neighboring cells could complicate their motility behavior. From these cell tracks, two parameters, path length (L) and displacement (D), were computed (Fig. 4 C). Dividing L and D by the total trajectory time (t) yielded mean movement speed and velocity (a measure of productive displacement rate), respectively. Comparison of these parameters indicated that the average movement speeds between cells of the two genotypes were similar (Fig. 4 D), but the wild-type cells moved with a considerably higher velocity (Fig. 4 E). Thus, although wild-type and mutant cells were similarly motile, the motility of mutant cells did not lead to displacement efficiently. The D/L ratio is a measure of the straightness of each cell track and showed that the paths of ARPC3$^{-/-}$ fibroblasts were significantly less straight than those of wild-type cells (Fig. 4 F). This result suggests that the mutant cells have a deficiency in sustaining the directionality of the movement.

To assess this further, we performed a mean square displacement (MSD) analysis of the cell-tracking data. The MSD was calculated using the equation:

$$MSD(\tau) = \left\langle \left| \vec{r}(t+\tau) - r(t) \right|^2 \right\rangle,$$

where $\vec{r}(t)$ is the position of the cell at time t. The result was fitted to $MSD(\tau) = 4D\tau^{\alpha}$, where D is the diffusion coefficient and the exponent α indicates the degree of directional motion. The resulting average MSD curve for wild-type cells showed an upward trend and the corresponding α value was 1.43 ± 0.05, indicating directional motion, whereas the MSD plot for the mutant cells was nearly linear with an α value of 1.09 ± 0.09, not significantly deviating from $\alpha = 1$ for pure random walk (P-value = 0.14; Fig. 4, G and H). Consistent with these quantitative analyses, observation of cell movement in the time-lapse movies also gave the impression that the mutant cells had a reduced ability to maintain a consistent leading edge (compare Videos 3 and 4), possibly as a result of the independently protruding and retracting FLPs, as opposed to the apparently more coordinated dynamics of lamellipodia of ARPC3$^{+/+}$ cells. To assess the level of coordination at the leading edge, we calculated the spatial (angular) correlations of leading edge protrusion and retraction dynamics in the migrating ARPC3$^{+/+}$ and ARPC3$^{-/-}$ cells from the kymographs in Fig. 3 (see Materials and methods for details). This analysis found the amplitude of the correlation to be in general much higher in the wild-type cells than in the mutant cells (Fig. 3 F), and the characteristic angular distance for correlation decay was also larger in the wild type than that in the mutant (Fig. 3 G). This analysis indicates poor coordination of protrusion and retraction dynamics at the mutant cell leading edge and provides a possible explanation for the lack of directional persistence in the movement of ARPC3$^{-/-}$ fibroblasts.

ARPC$^{-/-}$ fibroblasts are defective in chemotaxis in response to an EGF gradient

Because the environment in a wound-healing assay is complex and the cells may not be experiencing a robust directional cue, we further tested the ability of ARPC3$^{-/-}$ fibroblasts to undergo directional migration in a chemotaxis assay along a gradient of EGF. We first tested the ability of ARPC3$^{+/+}$ and ARPC3$^{-/-}$ cells to respond to uniform EGF. Wild-type fibroblasts responded within minutes of EGF (25 ng/ml) stimulation with slightly but apparently more vigorous lamellipodia protrusions and retractions (Video 7), and interestingly, this response was even more

Published April 9, 2012

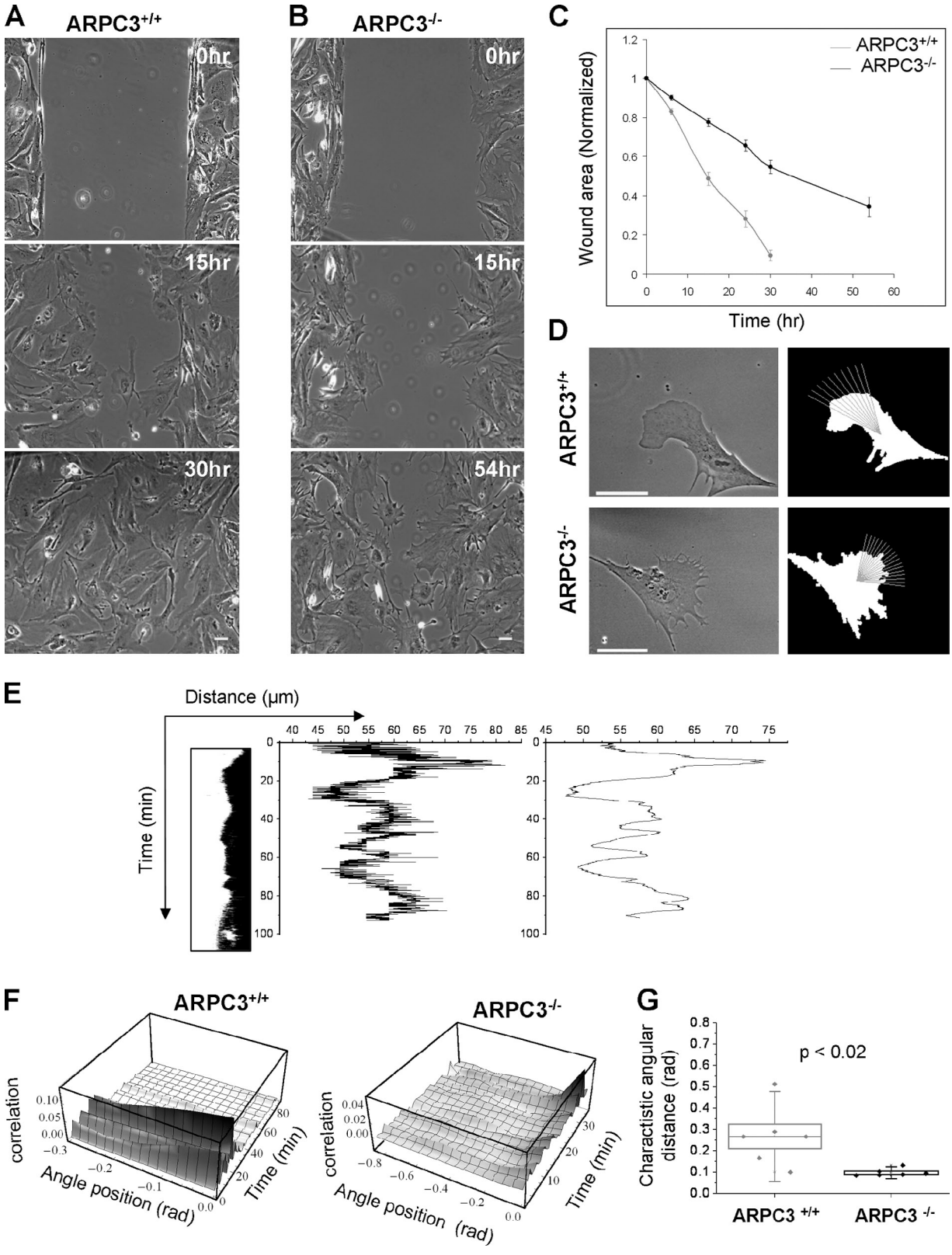

Figure 3. **ARPC3$^{-/-}$ fibroblast cells in wound healing and their leading edge dynamics.** (A and B) Wound-healing montage of ARPC3$^{+/+}$ and ARPC3$^{-/-}$ fibroblast cells. Bars, 50 µm. (C) Quantification of wound area as a function of time. Plots show mean and standard deviation from six different regions along the wound per experiment and three experiments per genotype. (D) Cell boundary segmentation and illustration of leading edge kymograph line selection. Bars, 25 µm. (E) Each kymograph (left) was digitized (center) and then smoothed for assignment of protrusion and retraction segments. (F) Angular correlation functions were computed as described in Materials and methods. (G) The smaller width at half maximum of the angular correlation function for mutant indicates less coordinated motion of the leading edge than for wild type. Small box shows the mean, line shows median, large box the SEM, and whiskers show SD.

Published April 9, 2012

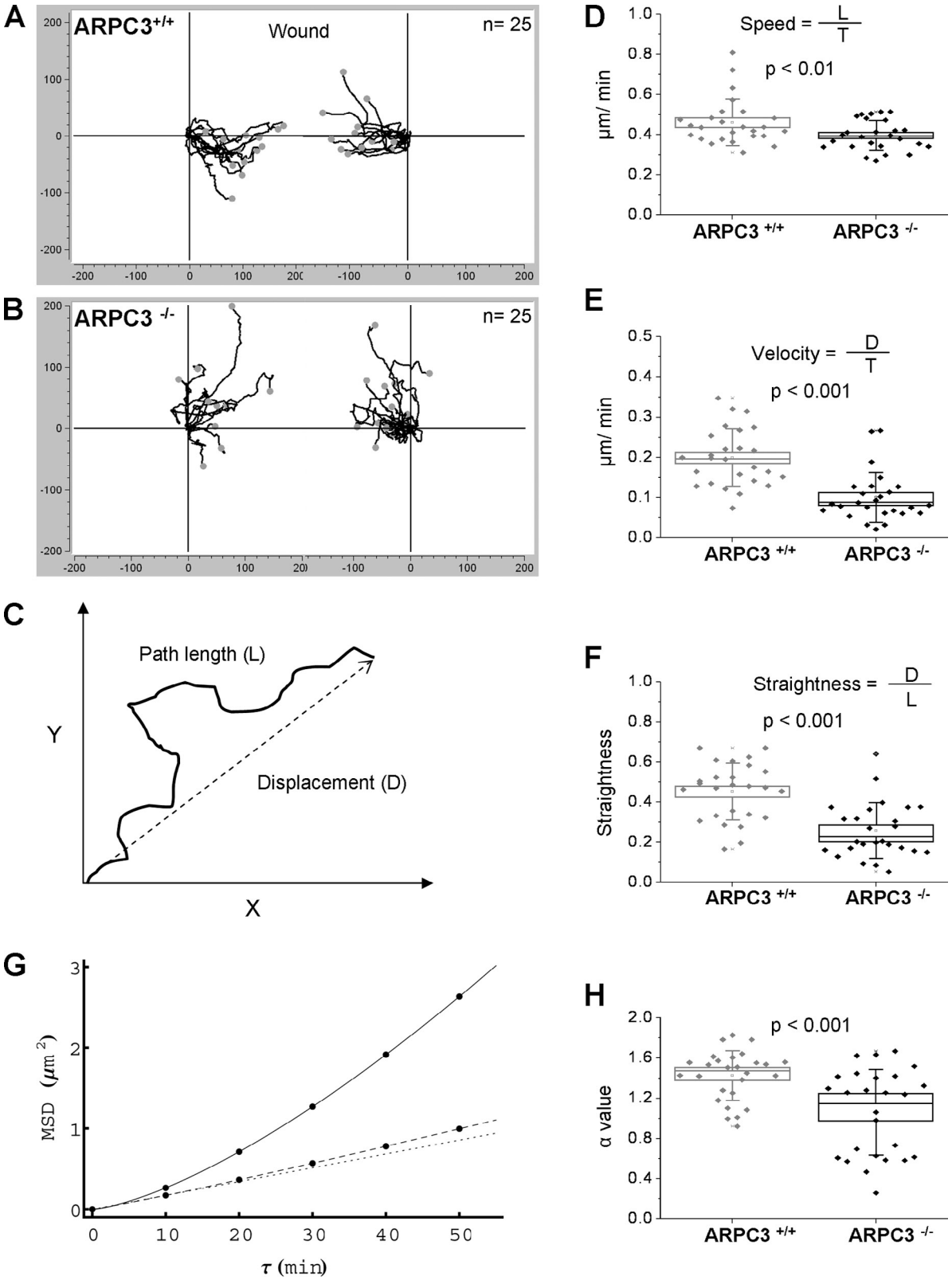

Figure 4. **Migration behavior of individual ARPC3$^{+/+}$ and ARPC3$^{-/-}$ fibroblast cells during wound closure.** (A and B) Aggregated trajectories of ARPC3$^{+/+}$ (A) and ARPC3$^{-/-}$ (B) fibroblast cells migrating for 10 h toward the wound center. (C) Visual demonstration of path length vs. displacement for speed and velocity calculations. (D) Cell speed, (E) velocity, and (F) straightness of wild-type and mutant cells. Notation is as in Fig. 3 G. (G) A plot of MSD vs. time shift and (H) α values from MSD curve fits indicating more directed motion for ARPC3$^{+/+}$ cells (solid line) than for ARPC3$^{-/-}$ cells (dashed line). Dotted line represents the case for $\alpha = 1$ indicating pure random motion.

Published April 9, 2012

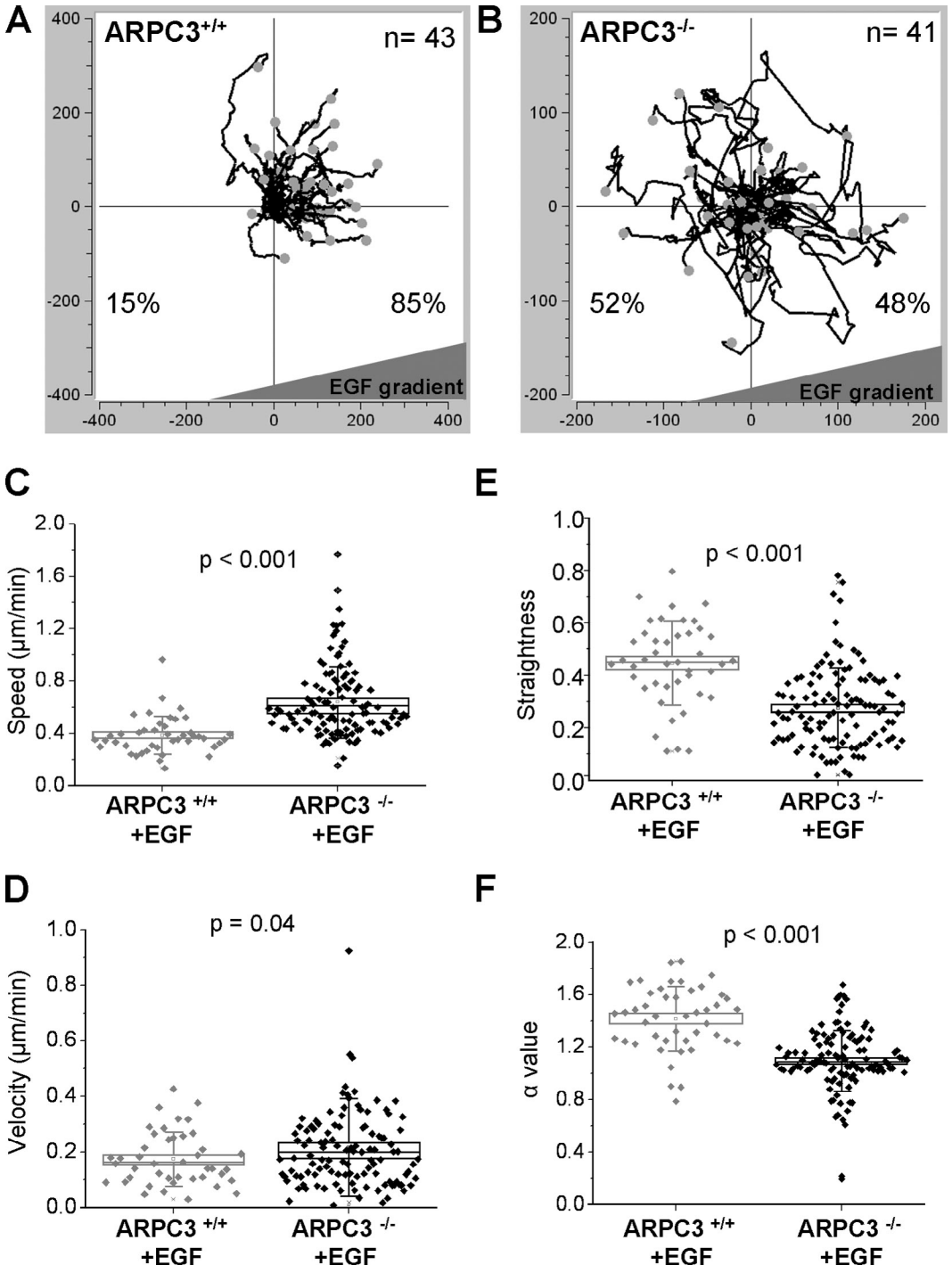

Figure 5. **Chemotaxis of ARPC3$^{+/+}$ and ARPC3$^{-/-}$ fibroblast cells in response to an EGF gradient.** The ARPC3$^{+/+}$ and ARPC3$^{-/-}$ cells were plated on fibronectin-coated µ-Slide and analyzed for 12 h in the presence of EGF gradient (500 ng/ml at source). (A and B) Aggregated trajectories of individual ARPC3$^{+/+}$ (A) and ARPC3$^{-/-}$ (B) cells in the presence of the EGF gradient. (C) Cell speed, (D) velocity, (E) straightness, and (F) MSD α values for wild-type and mutant cells presented as in Fig. 4. The data came from tracking of 43 (two experiments) ARPC3$^{+/+}$ and 115 (five experiments) ARPC3$^{-/-}$ cells.

pronounced in ARPC3$^{-/-}$ cells (Video 8, Table S2). A stable EGF gradient was established by using the microfluidics device µ-Slide (Ibidi; see Materials and methods). The motility of cells in the presence of the EGF gradient was tracked for 12 h. ARPC3$^{+/+}$ cells migrated up the gradient as expected, with 85% of cells moving closer to the EGF source at the end of the observation (Fig. 5 A, Video 9). By contrast, the mutant cells failed chemotaxis with only 48% cells moving closer to the EGF source (Fig. 5 B, Video 10). Analysis of the parameters describing single cell movement (as in Fig. 4) found again that the mutant cells failed to sustain movement directionality and exhibited mostly random walk in the presence of the EGF gradient (Fig. 5, C–F).

Taken together, the analysis of ARPC3$^{-/-}$ fibroblasts in comparison with ARPC3$^{+/+}$ fibroblasts described above

Published April 9, 2012

provides the functional evidence supporting the notion that the Arp2/3 complex plays a critical role in the formation of lamellipodia. However, without the Arp2/3 complex the fibroblasts cells were still able to form dynamic membrane protrusions with filopodia-like morphology. Detailed ultrastructural analysis will be necessarily to determine if the FLPs observed in ARPC3$^{-/-}$ fibroblasts are indeed the stereotypical filopodia (Resch et al., 2002; Svitkina et al., 2003; Korobova and Svitkina, 2008), and future work with other Arp2/3 complex subunit mutants should help ascertain that ARPC3$^{-/-}$ represents complete Arp2/3 complex null. Interestingly, a recent study found that WAVE and the Arp2/3 complex jointly inhibits mDia2-mediated filopodia formation through a physical interaction with mDia2 (Beli et al., 2008), providing a possible explanation of the abundant FLP formation and prominent localization of DRF proteins at the tip of these processes in ARPC3$^{-/-}$ cells.

A surprising result of our study is that ARPC3$^{-/-}$ cells are capable of rapid spreading and are highly motile despite the lack of lamellipodia. The mutant fibroblasts exhibited a movement speed comparable to (in wound healing) or even faster than (in the presence of EGF) that of wild-type fibroblasts. This correlates with more vigorous FLP dynamics (higher protrusion and retraction rates) at the leading edge of the mutant fibroblasts than those at the leading edge of lamellipodia in wild-type cells. However, a glaring defect of the mutant cells was their inability to undergo persistent directional movement, leading to a considerable delay in wound healing compared with wild-type cells. We speculate that this deficiency may be intrinsic to the FLP-based leading edge. Correlation analysis found poor coordination in the protrusion and retraction dynamics between neighboring positions on the leading edge in the mutant cells, possibly as a consequence of independent nucleation, elongation, and retraction of individual FLPs. This lack of coordination could possibly increase the chance of stochastic switch of the directionality of leading edge extension. By contrast, the protrusion and retraction dynamics are highly coordinated along the leading edge of ARPC3$^{+/+}$ fibroblasts, likely as a consequence of the auto-catalytic, dendritic actin nucleation mediated by the Arp2/3 complex, whereby the nucleation of a new filament is favored in the vicinity of other elongating actin filaments at the leading edge. This finding suggests that Arp2/3 complex-mediated lamellipodia extension may be particularly favorable to cell migration processes that require strong directional persistence.

Using a chemotaxis assay in the presence of an EGF gradient, we found that ARPC3$^{-/-}$ fibroblasts are deficient in directional cell migration even in the presence of a stable directional cue. The explanation for this defect may be more complex than that for the delayed wound healing. Although a lack of leading edge coordination could contribute to frequent turning from the expected direction, a lack of any observable bias in cell movement may suggest that the cell's ability to recognize and amplify the external gradient was also disrupted in the absence of Arp2/3-mediated actin assembly. The ARPC3$^{-/-}$ cells were able to respond to EGF stimulation by forming more dynamic FLPs, but a failure in gradient sensing in these cells could be due to the disruption of a feedback loop from the Rac–Arp2/3 pathway of actin assembly to the upstream signaling events, which in neutrophils plays an important role in amplifying the directional cue from chemoattractant gradient (Glogauer et al., 2000; Wang et al., 2002; Weiner et al., 2002; Sun et al., 2007).

In summary, using mouse gene-disruption technology and ES cell differentiation we have performed a detailed analysis comparing the motility behavior of fibroblast cells in the presence or absence of a functional Arp2/3 complex. Our results demonstrate a critical role for the Arp2/3 complex in the assembly of lamellipodia-based leading edges and directional cell motility. As ES cells can be differentiated into a wide array of motile cells such as neutrophils, dendritic cells, and neurons (Fairchild et al., 2000; Bibel et al., 2004; Lieber et al., 2004), the model system established in this work should be useful for dissecting the function of the Arp2/3 complex in motile cells and unraveling the evolution design principles in the machineries that drive diverse cell motility processes.

Materials and methods

Generation and analysis of ARPC3$^{+/-}$ gene-trap mice

ES cell clone (XG476) carrying the ARPC3 gene disruption was purchased from the Bay genomics (version CC183108.1) and were injected into the blastocyst of the C57BL6 blastocysts (3.5 dpc) with Nikon micromanipulators. The blastocysts were cultured in KSOM+AA for 2–3 h and were transplanted into the uterus of 2.5(dpc) pseudo-pregnant recipient F1 mothers (CBAXC57Bl/10). The offspring born with agouti coat color reflect the contribution of the ES cells to the developing embryo. Successful transmission of the mutation was initially determined by mating the chimeras to wild-type C57BL/6 females. Offspring with agouti coat color represent the transmission of the 129 ES cell background and were genotyped to identify the presence of the mutated allele. The mouse line was further established by intercrossing the heterozygous male and females. The ARPC3$^{+/-}$ line was established by backcrosses with mice of the C57BL/6 genetic background.

ARPC3$^{+/+}$, ARPC3$^{+/-}$, and ARPC3$^{-/-}$ ES cell derivation and maintenance

ARPC3$^{+/-}$ females (4–8 wk old) were mated with (ARPC3$^{+/-}$) males. The uterine horns and uterus were dissected from the 3.5-d pregnant female mice and the blastocysts were collected in M2 medium and washed and cultured in a drop of KSOM+AA media overlaid with mineral oil at 37°C in a humidified atmosphere with 5% CO_2. ES cell derivation was performed with slight modification of the protocols described previously (Egli et al., 2007). In brief, blastocyst zonae pellucidae was removed by treating with acidic Tyrode's solution (Millipore) and washed with KSOM+AA medium. The blastocysts were transferred individually into individual wells of 4-well IVF plates (Thermo Fisher Scientific) coated with 0.1% (wt/vol) gelatin and filled with a layer of iMEF (Global Stem) in 500 µl of ES cell derivation medium. This medium contains Knockout DMEM (Invitrogen), 20% Knockout FBS (Invitrogen), 2 mM L-glutamine (Invitrogen), 50 U/ml penicillin/50 µg/ml streptomycin (Invitrogen), 0.1 mM β-mercaptoethanol (BD), 0.1 mM MEM nonessential amino acids (Invitrogen), 1,000 U/ml recombinant mouse LIF (Millipore), and mitogen-activated protein kinase inhibitor (PD98059; Cell Signaling Technology) at 37°C in an incubator with 5% CO_2. The blastocysts were allowed to attach to the iMEF feeder layer without disturbance for 6 d and cultured up to 12 d by changing the ES derivation medium every second day. The inner cell mass was mechanically detached using a glass pipette tip and transferred into a 12-well plate containing iMEFs. The ES cell colonies were cultured further, washed with calcium- and magnesium-free PBS, and trypsinized with 0.25% trypsin/EDTA for 2–5 min at 37°C. The cells were centrifuged and transferred into a 6-well plate and cultured in Knockout DMEM-FBS medium until they were confluent. At this stage, each ES clone was plated in duplicates in 6-well plates with one set being used for genotyping and the other for further colony expansion. To scale up the ES cell culture, cells were cultured in T75 flasks filled with iMEF and Knockout DMEM-FBS medium until they reached 70–80% confluence. The ES cells were frozen in 10% DMSO and 90% FBS and stored in liquid nitrogen.

ES cell differentiation into fibroblast using retinoic acid

ARPC3$^{+/-}$ and ARPC3$^{-/-}$ ES cells were separated from the iMEFs by transferring into a new dish every 45 min, taking advantage of the fact that

Published April 9, 2012

iMEFs are more adherent. The ES cells in supernatant were spun down at 1,000–1,200 rpm for 5 min and used either for genotyping or differentiation. The ES cells were seeded into pregelatin-coated T75 flask(s) or 150-mm dishes with ES cell medium containing LIF. Cells were allowed to settle down on plates overnight and replaced with fibroblast medium (DMEM high-glucose [Invitrogen], 10% FBS, 1% nonessential amino acids [Invitrogen], 0.1% 2-mercaptoethanol, 50 U/ml penicillin, and 50 µg/ml streptomycin) containing 3.33×10^{7} M (0.33 µM) retinoic acid (Smith, 1991). The media was changed twice at 24-h intervals. Cells were cultured for up to 7 d, with daily changes of medium after the initial 72 h. Undifferentiated ES cells were separated from the fibroblasts by consecutive transfer to a new dish every 30 min. The fibroblast cells re-adhere to the substrate faster than the undifferentiated ES cells. The differentiated fibroblast cells were able to survive for ∼10 d after 7 d of differentiation and 2–3 passages.

Genotyping of ARPC3$^{+/+}$ and ARPC3$^{-/-}$ ES cells and fibroblast cells and RT-PCR

Genomic DNA from ARPC3$^{+/+}$, ARPC3$^{+/-}$, and ARPC3$^{-/-}$ ES cells and fibroblast cells was isolated by homogenizing the cells in 20–40 µl extraction buffer and 5–10 µl tissue preparation buffer (Sigma-Aldrich). Homogenized samples were incubated for 20 min at room temperature, 5 min at 95°C, and then neutralized with 20–40 µl of neutralization buffer. The supernatant was used for the PCR genotyping using Red extract PCR mixture (Sigma-Aldrich) with the following primers: P1: ARPC3-Wt-F 5′-TGCAGGCATACCACTCTTCTCTCA-3′; P2: ARPC3-Wt-R 5′-AGCACCACGAATTGAGGCTAGAGT-3′; and P3: ARPC3-GT-R 5′-AAAGGGTCTTTGAGCACCAGAGGA-3′.

RT-PCR analysis in fibroblast cells was performed by isolating the total RNA from ARPC3$^{+/+}$, ARPC3$^{+/-}$, and ARPC3$^{-/-}$ fibroblasts using an RNA extraction kit (QIAGEN). cDNA was synthesized from total RNA using Superscript III (Invitrogen) reverse transcription with random hexamer primers (Invitrogen). To examine the expression of ARPC3 wild-type or gene-trap truncated mRNA, cDNA was amplified using the following primers: P4: Xg476-wt-E2F 5′-GGACACCAAGCTCATCGGTAACAT-3′; P5: Xg476-wt-E4R 5′-GATGTAGATCAATGTCCTGTCCGC-3′; and P6: Xg476-βgeo-R 5′-ATTCAGGCTGCGCAACTGTTGGG-3′.

Immunofluorescence staining

ARPC3$^{+/-}$, ARPC3$^{+/-}$, and ARPC3$^{-/-}$ ES cells were cultured on a 0.1% (wt/vol) gelatin-coated glass-bottom dish for 3 d. Cells were washed and fixed with 4% paraformaldehyde in PBS for 25 min. Fixed cells were permeabilized by treatment with PBS/0.1% Tween 20 for 5 min and blocked by incubation with 3% BSA in PBS for 1 h. Cells were then incubated in PBS with 3% BSA containing Oct4 antibodies (mouse; Abcam) at a dilution of 1:100 overnight at 4°C. Cells were washed three times with PBS/0.1% Tween 20 and then incubated for 1 h with Alexa 488–conjugated mouse anti–rabbit secondary antibody at a dilution of 1:300 for 45 min at 37°C. Cells were washed with PBS/ 0.1% Tween 20 and then counterstained with fluorescent phalloidin (Invitrogen) for actin filaments and DAPI for DNA. The cells were mounted and imaged under a confocal microscope (LSM-510-LIVE; Carl Zeiss).

ARPC3$^{+/+}$ and ARPC3$^{-/-}$ fibroblast cells were grown on glass coverslips (or) glass-bottom dishes for 24 h. Two different fixation protocols were used. For staining IB10, Arp2, and mDia1, the cells were fixed with 4% paraformaldehyde in PBS at 37°C for 30 min. After fixation and permeabilization as described above, cells were blocked with fetal bovine serum or 3% BSA for 1 h and incubated with the primary antibodies against: IB10 (1:75; Abcam), Arp2 (1:200 and 1:75 for two different batches; Santa Cruz Biotechnology, Inc.), ARPC3 (1:50; BD), and mDia1 (1:200; Santa Cruz Biotechnology, Inc.) overnight at 4°C. After three washes with PBS/ 0.2% Tween 20, the cells were incubated with a corresponding secondary antibody coupled to Alexa Fluor 488 (Invitrogen) at a dilution of 1:300 at 37°C for 1 h. Cells were washed with PBS/0.2% Tween 20 and then counterstained with Alexa Fluor 546 phalloidin (Invitrogen) and DAPI. For straining with anti-mDia2 (a gift from Dr. S. Narumiya, Kyoto University, Kyoto, Japan), cells were fixed with 10% TCA on ice for 15 min as described in Watanabe et al. (2008). The fixed cells were washed with PBS containing 30 mM glycine (G-PBS) and permeabilized with 0.2% Tween 20 in G-PBS for 5 min on ice, followed by three washes with G-PBS and processed as described above. For fascin antibody (1:50; Millipore) staining, the cells were fixed with methanol at −20°C for 15 min.

Alkaline phosphatase assay

ARPC3$^{+/-}$, ARPC3$^{+/-}$, and ARPC3$^{-/-}$ ES cells were cultured and fixed with 4% paraformaldehyde in PBS for 30 min at 37°C. Cells were washed in PBS and incubated with recommended substrate solutions (Vector Laboratories) for 20–30 min at room temperature until sufficient staining developed. Cells were imaged under a microscope (Axiovert; Carl Zeiss) using Plan Neofluor 10x/0.30 Ph1 (DIC I) 10x objectives.

Cell spreading and wound-healing assays

For observing cell spreading, ARPC3$^{+/+}$ and ARPC3$^{-/-}$ fibroblast cells were trypsinized with 0.05% trypsin/EDTA for 5 min and centrifuged. The cells were resuspended in fibroblast medium and placed on a glass-bottom dish (MatTek Corp.) coated with 5 µg/ml of bovine fibronectin (Sigma-Aldrich) for 20 min in a 37°C incubator. The cell spreading was recorded on a microscope equipped with a 37°C incubator and 5% CO_2 for a period of 2 h with frames taken every 2 min. Phase-contrast imaging was performed either with a microscope (LSM-510; Carl Zeiss) equipped with a Plan-Apochromat 20x/0.6 Ph2 air objective (Carl Zeiss) or with a microscope (Eclipse TE2000-E; Nikon) equipped with a Plan-Fluar 10x Ph1 DLL objective and a CCD camera (CoolSNAP; Photometrics). For the LSM-510 microscope, images were collected using the maximum field of view and 512 × 512 image size. The overall spreading area was measured by outlining the cell boundary every 10 frames using custom ImageJ segmentation software (described below).

For the wound-healing assay, ARPC3$^{+/+}$ and ARPC3$^{-/-}$ fibroblast cells were cultured in fibroblast medium as described previously. Glass-bottom dishes were coated with 5 µg/ml fibronectin at 37°C for 1–2 h, washed with PBS, and attached to a culture insert (Ibidi). Fibroblast cells were trypsinized with 0.05% trypsin for 5 min, centrifuged, and resuspended in fibroblast medium. The cells suspensions (85 µl) were seeded at a density of $1.5–2.0 \times 10^{5}$ cells/ml and cultured overnight at 37°C with 5% CO_2. The next day, cells were rinsed with PBS at least twice and switched to DMEM with 0.5% serum for 12 h. The culture insert was removed to create the "wound", and cells were rinsed with PBS and fed with fibroblast culture medium supplemented with 10% FBS. The wounds were imaged with phase contrast on the LSM-510 microscope using a Plan-Neofluar 10x/0.30 Ph1 objective at different time points, and healing was quantified by manually measuring the wound areas that remained using Axiovision software (Carl Zeiss). For the cell-tracking analysis movies were made for 10 h with frames taken every 10 min; leading edge dynamics movies were 1.5 h long with an interval of 3 s/frame.

Chemotaxis assay

Chemotaxis was assayed following Ibidi protocol with several modifications. In brief, ARPC3$^{+/+}$ and ARPC3$^{-/-}$ fibroblast cells were trypsinized and counted. The cell suspension was diluted to $\sim 3 \times 10^{6}$ cells/ml. The µ-Slide Chemotaxis slides (Ibidi) were coated with 5 µg/ml of fibronectin at 37°C for 1–2 h and washed with PBS. The C, D, E, and F ports were closed with plugs and 6 µl of cell suspension was applied onto filling port (A) of the µ-Slide using a 20-µl pipettor and 6 µl of air was aspirated from the opposite filling port (B). The slide was placed in a sterile 10-cm Petri dish with a wet tissue around the slide and incubated in the tissue culture hood for 15 min and transferred to a 37°C incubator until the cells were attached. All plugs were gently removed from the filling ports and both reservoirs were filled with 70 µl chemoattractant-free medium. One of the filling ports was filled with 18 µl chemoattractant (500 ng/ml EGF) solution by removing 18 µl of medium from the other port on the same side of the device. Once again, all the ports were closed with plugs. Cell migration was recorded by mounting the µ-Slide on the stage of an inverted microscope with a 37°C incubator and 5% CO_2. For the trajectory analysis, movies were made using the LSM-510 microscope with an A-Plan10x/0.25 Ph1 air objective or the Eclipse TE2000-E microscope as described above for a period of 12 h with frames taken every 10 min.

Cell trajectory analysis

Movies were acquired on an inverted microscope as described above in the wound-healing and chemotaxis assay sections. To generate the trajectories for the wound-healing assay, single cells at the wound edge were tracked by manually selecting the nucleus throughout the movie using a custom plug-in written for ImageJ (National Institutes of Health [NIH], Bethesda, MD). For the chemotaxis assay, single cells were tracked by selecting the center of mass throughout the length of the movie using the Chemotaxis and Migration tool for ImageJ from Ibidi. For both assays, speed, velocity, straightness, and α value were obtained by using Mathematica software (Wolfram Research Inc.). The trajectory path length and the displacement from the initial to the end point of each trajectory was computed. The speed and mean velocity are given by the ratio of the path length and the displacement to the total trajectory time, respectively. The trajectory straightness is computed as the ratio of displacement to path length. The mean

Published April 9, 2012

squared displacement was found for each trajectory according to the following formula:

$$MSD(\tau) = \left\langle \left| \vec{r}(t+\tau) - \vec{r}(t) \right|^2 \right\rangle,$$

where $\vec{r}(t)$ is the two-dimensional position at time t, and < > denotes time averaging. This quantity was fit by nonlinear least squares to the following general formula: $MSD(\tau) = 4D\tau^{\alpha}$, where D is the apparent diffusion coefficient and α is a factor indicating nonrandom diffusion. For purely random motion (e.g., Brownian diffusion), α is 1 and MSD follows a straight line. For directed motion, α is greater than 1, and for confined motion α is smaller than 1.

Cell segmentation

For analysis methods involving leading edge tracking (cell spreading or leading edge dynamics), phase-contrast images were segmented using a custom plug-in written for ImageJ, which links to the OpenCV library (Willow Garage) following the example of the CellTrack program (Sacan et al., 2008). In brief, each phase-contrast image frame was processed by first performing Canny edge detection followed by a single binary dilation. Subsequently, the binary image was outlined using the cvFindContours subroutine of OpenCV. Finally, the outline containing the largest area was selected and filled to create a cell mask.

Kymograph analysis

For the kymograph analysis of leading edge dynamics, phase-contrast time-lapse movies were made with the LSM-510 microscope using a Plan-Apochromat 20x/0.6 Ph2 air objective for a period of 1.5 h with frames taken every 3 s. The cells chosen for analysis were single cells migrating in the wound. These cells were cropped from the full-size images and the leading edge boundary was masked frame by frame (see above) to reduce noise without altering the position of the cell edge. Masked images were further processed by automatic generation of several equally spaced (5° in angular measure) 1-pixel-wide lines from a manually chosen central point to the leading edge of the cell and subsequent calculation of the distance to the leading edge along each line in the direction of individual protrusions using a custom-written ImageJ plug-in. We note that the protrusion and retraction rate determined using this plug-in was confirmed by those determined with manual kymographs of the FLPs in the mutant cells. The distances generated above were subsequently analyzed using Mathematica software. Each kymograph was smoothed using a moving averaging window of 30 time points and regions of leading edge protrusion and retraction were determined as follows. First, the smoothed kymograph was segmented into 10 time point segments. The slopes of these segments were calculated from the starting and ending points of the segments. Slopes between 10% and −10% of the maximal and minimal slope for each trajectory were eliminated. Segments with contiguous regions with slopes of the same sign were flagged as protruding (positive slope) or retracting (negative slope). The durations and average slopes of these contiguous regions were averaged to give the final duration and rate measurements for each trajectory. In addition, for each time step the angular correlation $C(\psi)$ of the leading edge dynamics was computed. This quantity is defined as:

$$C(\psi) = \langle v(\varphi)v(\varphi - \psi) \rangle,$$

where $v(\phi)$ is the velocity as a function of angular position ϕ along the leading edge, ψ is the angular shift, and < > denotes averaging over ϕ. If the adjacent regions of the leading edge are concerted in velocity the width of the angular correlation function (at half of its maximal value) is large, whereas for uncorrelated velocity distributions this width tends to zero.

Online supplemental material

Fig. S1 shows generation of ARPC3$^{+/-}$ gene-trap mouse and ARPC3$^{+/+}$ and ARPC3$^{-/-}$ ES cells. Fig. S2 shows characterization of ARPC3$^{+/+}$ and ARPC3$^{-/-}$ ES cells. Fig.S3 shows characterization of ARPC3$^{+/+}$ and ARPC3$^{-/-}$ fibroblast cells by immunofluorescence staining. Video 1 shows a spreading ARPC3$^{+/+}$ fibroblast cell. Video 2 shows a spreading ARPC3$^{-/-}$ fibroblast cell. Video 3 shows ARPC3$^{+/+}$ fibroblast cells migrating toward the wound. Video 4 shows ARPC3$^{-/-}$ fibroblast cells migrating toward the wound. Video 5 shows trajectories of individual ARPC3$^{+/+}$ fibroblast cells during wound closure. Video 6 shows trajectories of individual ARPC3$^{-/-}$ fibroblast cells. Video 7 shows ARPC3$^{+/+}$ fibroblast cells responding to stimulation with 25 ng/ml EGF. Video 8 shows ARPC3$^{-/-}$ fibroblast cells responding to stimulation with 25 ng/ml EGF. Video 9 shows trajectories of individual ARPC3$^{+/+}$ fibroblast cells migrating in the presence of an EGF gradient. Video 10 shows trajectories of individual ARPC3$^{-/-}$ cells migrating in the presence of an EGF gradient. Table S1 shows leading edge protrusion and retraction rates and durations. Table S2 shows quantification of leading edge dynamics. Online supplemental material is available at http://www.jcb.org/cgi/content/full/jcb.201112113/DC1.

We thank K. Eggan and D. Egli for advice on ES cell derivation; B. Slaughter for assisting with imaging; K. Westfahl for mice maintenance; N. Shuh and S. Watanabe for providing the anti-mDia2 antibody; T. Svitkina for advice on fascin staining; and Ana Pedraza and Henrietta Szutorisz for advice on fibroblast differentiation. This study was done to fulfill, in part, requirements for P. Suraneni's PhD thesis as a student registered with the Open University.

This work was supported by NIH grant P01 GM066311.

Submitted: 20 December 2011
Accepted: 14 March 2012

References

Abercrombie, M., and J.E.M. Heaysman. 1954. Observations on the social behaviour of cells in tissue culture. II. Monolayering of fibroblasts. *Exp. Cell Res.* 6:293–306. http://dx.doi.org/10.1016/0014-4827(54)90176-7

Abercrombie, M., J.E.M. Heaysman, and S.M. Pegrum. 1971. The locomotion of fibroblasts in culture. IV. Electron microscopy of the leading lamella. *Exp. Cell Res.* 67:359–367. http://dx.doi.org/10.1016/0014-4827(71)90420-4

Bailly, M., I. Ichetovkin, W. Grant, N. Zebda, L.M. Machesky, J.E. Segall, and J. Condeelis. 2001. The F-actin side binding activity of the Arp2/3 complex is essential for actin nucleation and lamellipod extension. *Curr. Biol.* 11:620–625. http://dx.doi.org/10.1016/S0960-9822(01)00152-X

Beli, P., D. Mascheroni, D. Xu, and M. Innocenti. 2008. WAVE and Arp2/3 jointly inhibit filopodium formation by entering into a complex with mDia2. *Nat. Cell Biol.* 10:849–857. http://dx.doi.org/10.1038/ncb1745

Bibel, M., J. Richter, K. Schrenk, K.L. Tucker, V. Staiger, M. Korte, M. Goetz, and Y.-A. Barde. 2004. Differentiation of mouse embryonic stem cells into a defined neuronal lineage. *Nat. Neurosci.* 7:1003–1009. http://dx.doi.org/10.1038/nn1301

Block, J., T.E.B. Stradal, J. Hänisch, R. Geffers, S.A. Köstler, E. Urban, J.V. Small, K. Rottner, and J. Faix. 2008. Filopodia formation induced by active mDia2/Drf3. *J. Microsc.* 231:506–517. http://dx.doi.org/10.1111/j.1365-2818.2008.02063.x

Bugyi, B., and M.F. Carlier. 2010. Control of actin filament treadmilling in cell motility. *Annu Rev Biophys*. 39:449–470. http://dx.doi.org/10.1146/annurev-biophys-051309-103849

Chhabra, E.S., and H.N. Higgs. 2007. The many faces of actin: matching assembly factors with cellular structures. *Nat. Cell Biol.* 9:1110–1121. http://dx.doi.org/10.1038/ncb1007-1110

Di Nardo, A., G. Cicchetti, H. Falet, J.H. Hartwig, T.P. Stossel, and D.J. Kwiatkowski. 2005. Arp2/3 complex-deficient mouse fibroblasts are viable and have normal leading-edge actin structure and function. *Proc. Natl. Acad. Sci. USA*. 102:16263–16268. http://dx.doi.org/10.1073/pnas.0508228102

Diegelmann, R.F., and M.C. Evans. 2004. Wound healing: an overview of acute, fibrotic and delayed healing. *Front. Biosci.* 9:283–289. http://dx.doi.org/10.2741/1184

Egli, D., J. Rosains, G. Birkhoff, and K. Eggan. 2007. Developmental reprogramming after chromosome transfer into mitotic mouse zygotes. *Nature*. 447:679–685. http://dx.doi.org/10.1038/nature05879

Fairchild, P.J., F.A. Brook, R.L. Gardner, L. Graça, V. Strong, Y. Tone, M. Tone, K.F. Nolan, and H. Waldmann. 2000. Directed differentiation of dendritic cells from mouse embryonic stem cells. *Curr. Biol.* 10:1515–1518. http://dx.doi.org/10.1016/S0960-9822(00)00824-1

Glogauer, M., J. Hartwig, and T. Stossel. 2000. Two pathways through Cdc42 couple the N-formyl receptor to actin nucleation in permeabilized human neutrophils. *J. Cell Biol.* 150:785–796. http://dx.doi.org/10.1083/jcb.150.4.785

Gournier, H., E.D. Goley, H. Niederstrasser, T. Trinh, and M.D. Welch. 2001. Reconstitution of human Arp2/3 complex reveals critical roles of individual subunits in complex structure and activity. *Mol. Cell*. 8:1041–1052. http://dx.doi.org/10.1016/S1097-2765(01)00393-8

Griffith, G.J., M.C. Trask, J. Hiller, M. Walentuk, J.B. Pawlak, K.D. Tremblay, and J. Mager. 2011. Yin-yang1 is required in the mammalian oocyte for follicle expansion. *Biol. Reprod.* 84:654–663. http://dx.doi.org/10.1095/biolreprod.110.087213

Gurtner, G.C., S. Werner, Y. Barrandon, and M.T. Longaker. 2008. Wound repair and regeneration. *Nature*. 453:314–321. http://dx.doi.org/10.1038/nature07039

Harris, E.S., T.J. Gauvin, E.G. Heimsath, and H.N. Higgs. 2010. Assembly of filopodia by the formin FRL2 (FMNL3). *Cytoskeleton (Hoboken)*. 67:755–772.

Higashida, C., T. Miyoshi, A. Fujita, F. Oceguera-Yanez, J. Monypenny, Y. Andou, S. Narumiya, and N. Watanabe. 2004. Actin polymerization-driven molecular movement of mDia1 in living cells. *Science*. 303:2007–2010. http://dx.doi.org/10.1126/science.1093923

Higgs, H.N., and T.D. Pollard. 1999. Regulation of actin polymerization by Arp2/3 complex and WASp/Scar proteins. *J. Biol. Chem.* 274:32531–32534. http://dx.doi.org/10.1074/jbc.274.46.32531

Kalluri, R., and M. Zeisberg. 2006. Fibroblasts in cancer. *Nat. Rev. Cancer*. 6:392–401. http://dx.doi.org/10.1038/nrc1877

Korobova, F., and T. Svitkina. 2008. Arp2/3 complex is important for filopodia formation, growth cone motility, and neuritogenesis in neuronal cells. *Mol. Biol. Cell*. 19:1561–1574. http://dx.doi.org/10.1091/mbc.E07-09-0964

Kreishman-Deitrick, M., C. Egile, D.W. Hoyt, J.J. Ford, R. Li, and M.K. Rosen. 2003. NMR analysis of methyl groups at 100-500 kDa: model systems and Arp2/3 complex. *Biochemistry*. 42:8579–8586. http://dx.doi.org/10.1021/bi034536j

Lee, J., J. Lee, E. Jung, Y.-S. Kim, K. Roh, K.-H. Jung, and D. Park. 2010. Ultraviolet A regulates adipogenic differentiation of human adipose tissue-derived mesenchymal stem cells via up-regulation of Kruppel-like factor 2. *J. Biol. Chem.* 285:32647–32656. http://dx.doi.org/10.1074/jbc.M110.135830

Lee, K., J.L. Gallop, K. Rambani, and M.W. Kirschner. 2010. Self-assembly of filopodia-like structures on supported lipid bilayers. *Science*. 329:1341–1345. http://dx.doi.org/10.1126/science.1191710

Lieber, J.G., S. Webb, B.T. Suratt, S.K. Young, G.L. Johnson, G.M. Keller, and G.S. Worthen. 2004. The in vitro production and characterization of neutrophils from embryonic stem cells. *Blood*. 103:852–859. http://dx.doi.org/10.1182/blood-2003-04-1030

Loisel, T.P., R. Boujemaa, D. Pantaloni, and M.-F. Carlier. 1999. Reconstitution of actin-based motility of *Listeria* and *Shigella* using pure proteins. *Nature*. 401:613–616. http://dx.doi.org/10.1038/44183

Machesky, L.M., and R.H. Insall. 1998. Scar1 and the related Wiskott-Aldrich syndrome protein, WASP, regulate the actin cytoskeleton through the Arp2/3 complex. *Curr. Biol.* 8:1347–1356. http://dx.doi.org/10.1016/S0960-9822(98)00015-3

Machesky, L.M., S.J. Atkinson, C. Ampe, J. Vandekerckhove, and T.D. Pollard. 1994. Purification of a cortical complex containing two unconventional actins from Acanthamoeba by affinity chromatography on profilin-agarose. *J. Cell Biol.* 127:107–115. http://dx.doi.org/10.1083/jcb.127.1.107

Machesky, L.M., E. Reeves, F. Wientjes, F.J. Mattheyse, A. Grogan, N.F. Totty, A.L. Burlingame, J.J. Hsuan, and A.W. Segal. 1997. Mammalian actin-related protein 2/3 complex localizes to regions of lamellipodial protrusion and is composed of evolutionarily conserved proteins. *Biochem. J.* 328:105–112.

Maly, I.V., and G.G. Borisy. 2001. Self-organization of a propulsive actin network as an evolutionary process. *Proc. Natl. Acad. Sci. USA*. 98:11324–11329. http://dx.doi.org/10.1073/pnas.181338798

May, R.C., M.E. Hall, H.N. Higgs, T.D. Pollard, T. Chakraborty, J. Wehland, L.M. Machesky, and A.S. Sechi. 1999. The Arp2/3 complex is essential for the actin-based motility of *Listeria monocytogenes*. *Curr. Biol.* 9:759–762. http://dx.doi.org/10.1016/S0960-9822(99)80337-6

Mullins, R.D., J.F. Kelleher, and T.D. Pollard. 1996. Actin' like actin? *Trends Cell Biol.* 6:208–212. http://dx.doi.org/10.1016/0962-8924(96)20017-0

Mullins, R.D., J.A. Heuser, and T.D. Pollard. 1998. The interaction of Arp2/3 complex with actin: nucleation, high affinity pointed end capping, and formation of branching networks of filaments. *Proc. Natl. Acad. Sci. USA*. 95:6181–6186. http://dx.doi.org/10.1073/pnas.95.11.6181

Nicholson-Dykstra, S.M., and H.N. Higgs. 2008. Arp2 depletion inhibits sheet-like protrusions but not linear protrusions of fibroblasts and lymphocytes. *Cell Motil. Cytoskeleton*. 65:904–922. http://dx.doi.org/10.1002/cm.20312

Pease, S., P. Braghetta, D. Gearing, D. Grail, and R.L. Williams. 1990. Isolation of embryonic stem (ES) cells in media supplemented with recombinant leukemia inhibitory factor (LIF). *Dev. Biol.* 141:344–352. http://dx.doi.org/10.1016/0012-1606(90)90390-5

Pellegrin, S., and H. Mellor. 2005. The Rho family GTPase Rif induces filopodia through mDia2. *Curr. Biol.* 15:129–133. http://dx.doi.org/10.1016/j.cub.2005.01.011

Peng, J., B.J. Wallar, A. Flanders, P.J. Swiatek, and A.S. Alberts. 2003. Disruption of the Diaphanous-related formin Drf1 gene encoding mDia1 reveals a role for Drf3 as an effector for Cdc42. *Curr. Biol.* 13:534–545. http://dx.doi.org/10.1016/S0960-9822(03)00170-2

Pollard, T.D. 2007. Regulation of actin filament assembly by Arp2/3 complex and formins. *Annu. Rev. Biophys. Biomol. Struct.* 36:451–477. http://dx.doi.org/10.1146/annurev.biophys.35.040405.101936

Pollard, T.D., and G.G. Borisy. 2003. Cellular motility driven by assembly and disassembly of actin filaments. *Cell*. 112:453–465. http://dx.doi.org/10.1016/S0092-8674(03)00120-X

Resch, G.P., K.N. Goldie, A. Krebs, A. Hoenger, and J.V. Small. 2002. Visualisation of the actin cytoskeleton by cryo-electron microscopy. *J. Cell Sci.* 115:1877–1882.

Rohatgi, R., L. Ma, H. Miki, M. Lopez, T. Kirchhausen, T. Takenawa, and M.W. Kirschner. 1999. The interaction between N-WASP and the Arp2/3 complex links Cdc42-dependent signals to actin assembly. *Cell*. 97:221–231. http://dx.doi.org/10.1016/S0092-8674(00)80732-1

Rønnov-Jessen, L., J.E. Celis, B. Van Deurs, and O.W. Petersen. 1992. A fibroblast-associated antigen: characterization in fibroblasts and immunoreactivity in smooth muscle differentiated stromal cells. *J. Histochem. Cytochem.* 40:475–486. http://dx.doi.org/10.1177/40.4.1552184

Rouiller, I., X.-P. Xu, K.J. Amann, C. Egile, S. Nickell, D. Nicastro, R. Li, T.D. Pollard, N. Volkmann, and D. Hanein. 2008. The structural basis of actin filament branching by the Arp2/3 complex. *J. Cell Biol.* 180:887–895. http://dx.doi.org/10.1083/jcb.200709092

Sacan, A., H. Ferhatosmanoglu, and H. Coskun. 2008. CellTrack: an open-source software for cell tracking and motility analysis. *Bioinformatics*. 24:1647–1649. http://dx.doi.org/10.1093/bioinformatics/btn247

Schaus, T.E., and G.G. Borisy. 2008. Performance of a population of independent filaments in lamellipodial protrusion. *Biophys. J.* 95:1393–1411. http://dx.doi.org/10.1529/biophysj.107.125005

Schaus, T.E., E.W. Taylor, and G.G. Borisy. 2007. Self-organization of actin filament orientation in the dendritic-nucleation/array-treadmilling model. *Proc. Natl. Acad. Sci. USA*. 104:7086–7091. http://dx.doi.org/10.1073/pnas.0701943104

Schirenbeck, A., T. Bretschneider, R. Arasada, M. Schleicher, and J. Faix. 2005. The Diaphanous-related formin dDia2 is required for the formation and maintenance of filopodia. *Nat. Cell Biol.* 7:619–625. http://dx.doi.org/10.1038/ncb1266

Singh, S.K., M.N. Kagalwala, J. Parker-Thornburg, H. Adams, and S. Majumder. 2008. REST maintains self-renewal and pluripotency of embryonic stem cells. *Nature*. 453:223–227. http://dx.doi.org/10.1038/nature06863

Smith, A.G. 1991. Culture and differentiation of embryonic stem cells. *Methods Cell Sci.* 13:89–94.

Stanford, W.L., J.B. Cohn, and S.P. Cordes. 2001. Gene-trap mutagenesis: past, present and beyond. *Nat. Rev. Genet.* 2:756–768. http://dx.doi.org/10.1038/35093548

Steffen, A., J. Faix, G.P. Resch, J. Linkner, J. Wehland, J.V. Small, K. Rottner, and T.E. Stradal. 2006. Filopodia formation in the absence of functional WAVE- and Arp2/3-complexes. *Mol. Biol. Cell*. 17:2581–2591. http://dx.doi.org/10.1091/mbc.E05-11-1088

Sun, C.X., M.A.O. Magalhães, and M. Glogauer. 2007. Rac1 and Rac2 differentially regulate actin free barbed end formation downstream of the fMLP receptor. *J. Cell Biol.* 179:239–245. http://dx.doi.org/10.1083/jcb.200705122

Svitkina, T.M., and G.G. Borisy. 1999. Arp2/3 complex and actin depolymerizing factor/cofilin in dendritic organization and treadmilling of actin filament array in lamellipodia. *J. Cell Biol.* 145:1009–1026. http://dx.doi.org/10.1083/jcb.145.5.1009

Svitkina, T.M., E.A. Bulanova, O.Y. Chaga, D.M. Vignjevic, S. Kojima, J.M. Vasiliev, and G.G. Borisy. 2003. Mechanism of filopodia initiation by reorganization of a dendritic network. *J. Cell Biol.* 160:409–421. http://dx.doi.org/10.1083/jcb.200210174

Thomson, J.A., J. Itskovitz-Eldor, S.S. Shapiro, M.A. Waknitz, J.J. Swiergiel, V.S. Marshall, and J.M. Jones. 1998. Embryonic stem cell lines derived from human blastocysts. *Science*. 282:1145–1147. http://dx.doi.org/10.1126/science.282.5391.1145

Tomasek, J.J., G. Gabbiani, B. Hinz, C. Chaponnier, and R.A. Brown. 2002. Myofibroblasts and mechano-regulation of connective tissue remodelling. *Nat. Rev. Mol. Cell Biol.* 3:349–363. http://dx.doi.org/10.1038/nrm809

Valkov, A., S.W. Sorbye, T.K. Kilvaer, T. Donnem, E. Smeland, R.M. Bremnes, and L.-T. Busund. 2011. The prognostic impact of TGF-β1, fascin, NF-κB and PKC-ζ expression in soft tissue sarcomas. *PLoS ONE*. 6:e17507. http://dx.doi.org/10.1371/journal.pone.0017507

Vignjevic, D., S.-i. Kojima, Y. Aratyn, O. Danciu, T. Svitkina, and G.G. Borisy. 2006. Role of fascin in filopodial protrusion. *J. Cell Biol.* 174:863–875. http://dx.doi.org/10.1083/jcb.200603013

Volkmann, N., K.J. Amann, S. Stoilova-McPhie, C. Egile, D.C. Winter, L. Hazelwood, J.E. Heuser, R. Li, T.D. Pollard, and D. Hanein. 2001. Structure of Arp2/3 complex in its activated state and in actin filament branch junctions. *Science*. 293:2456–2459. http://dx.doi.org/10.1126/science.1063025

Wang, F., P. Herzmark, O.D. Weiner, S. Srinivasan, G. Servant, and H.R. Bourne. 2002. Lipid products of PI(3)Ks maintain persistent cell polarity

and directed motility in neutrophils. *Nat. Cell Biol.* 4:513–518. http://dx.doi.org/10.1038/ncb810

Watanabe, S., Y. Ando, S. Yasuda, H. Hosoya, N. Watanabe, T. Ishizaki, and S. Narumiya. 2008. mDia2 induces the actin scaffold for the contractile ring and stabilizes its position during cytokinesis in NIH 3T3 cells. *Mol. Biol. Cell*. 19:2328–2338. http://dx.doi.org/10.1091/mbc.E07-10-1086

Weiner, O.D., P.O. Neilsen, G.D. Prestwich, M.W. Kirschner, L.C. Cantley, and H.R. Bourne. 2002. A PtdInsP(3)- and Rho GTPase-mediated positive feedback loop regulates neutrophil polarity. *Nat. Cell Biol.* 4:509–513. http://dx.doi.org/10.1038/ncb811

Welch, M.D., A.H. DePace, S. Verma, A. Iwamatsu, and T.J. Mitchison. 1997. The human Arp2/3 complex is composed of evolutionarily conserved subunits and is localized to cellular regions of dynamic actin filament assembly. *J. Cell Biol.* 138:375–384. http://dx.doi.org/10.1083/jcb.138.2.375

Welch, M.D., J. Rosenblatt, J. Skoble, D.A. Portnoy, and T.J. Mitchison. 1998. Interaction of human Arp2/3 complex and the *Listeria monocytogenes* ActA protein in actin filament nucleation. *Science*. 281:105–108. http://dx.doi.org/10.1126/science.281.5373.105

Wiles, M.V., F. Vauti, J. Otte, E.-M. Füchtbauer, P. Ruiz, A. Füchtbauer, H.-H. Arnold, H. Lehrach, T. Metz, H. von Melchner, and W. Wurst. 2000. Establishment of a gene-trap sequence tag library to generate mutant mice from embryonic stem cells. *Nat. Genet.* 24:13–14. http://dx.doi.org/10.1038/71622

Winter, D., A.V. Podtelejnikov, M. Mann, and R. Li. 1997. The complex containing actin-related proteins Arp2 and Arp3 is required for the motility and integrity of yeast actin patches. *Curr. Biol.* 7:519–529. http://dx.doi.org/10.1016/S0960-9822(06)00223-5

Winter, D.C., E.Y. Choe, and R. Li. 1999. Genetic dissection of the budding yeast Arp2/3 complex: a comparison of the in vivo and structural roles of individual subunits. *Proc. Natl. Acad. Sci. USA*. 96:7288–7293. http://dx.doi.org/10.1073/pnas.96.13.7288

Yae, K., V.W. Keng, M. Koike, K. Yusa, M. Kouno, Y. Uno, G. Kondoh, T. Gotow, Y. Uchiyama, K. Horie, and J. Takeda. 2006. Sleeping beauty transposon-based phenotypic analysis of mice: lack of Arpc3 results in defective trophoblast outgrowth. *Mol. Cell. Biol.* 26:6185–6196. http://dx.doi.org/10.1128/MCB.00018-06

Yang, C., and T. Svitkina. 2011. Visualizing branched actin filaments in lamellipodia by electron tomography. *Nat. Cell Biol.* 13:1012–1013, author reply :1013–1014. http://dx.doi.org/10.1038/ncb2321

Yang, C., L. Czech, S. Gerboth, S. Kojima, G. Scita, and T. Svitkina. 2007. Novel roles of formin mDia2 in lamellipodia and filopodia formation in motile cells. *PLoS Biol.* 5:e317. http://dx.doi.org/10.1371/journal.pbio.0050317

Yarar, D., W. To, A. Abo, and M.D. Welch. 1999. The Wiskott-Aldrich syndrome protein directs actin-based motility by stimulating actin nucleation with the Arp2/3 complex. *Curr. Biol.* 9:555–558. http://dx.doi.org/10.1016/S0960-9822(99)80243-7

Zigeuner, R., N. Droschl, V. Tauber, P. Rehak, and C. Langner. 2006. Biologic significance of fascin expression in clear cell renal cell carcinoma: systematic analysis of primary and metastatic tumor tissues using a tissue microarray technique. *Urology*. 68:518–522. http://dx.doi.org/10.1016/j.urology.2006.03.032

Published April 9, 2012

Suraneni et al., http://www.jcb.org/cgi/content/full/jcb.201112113/DC1

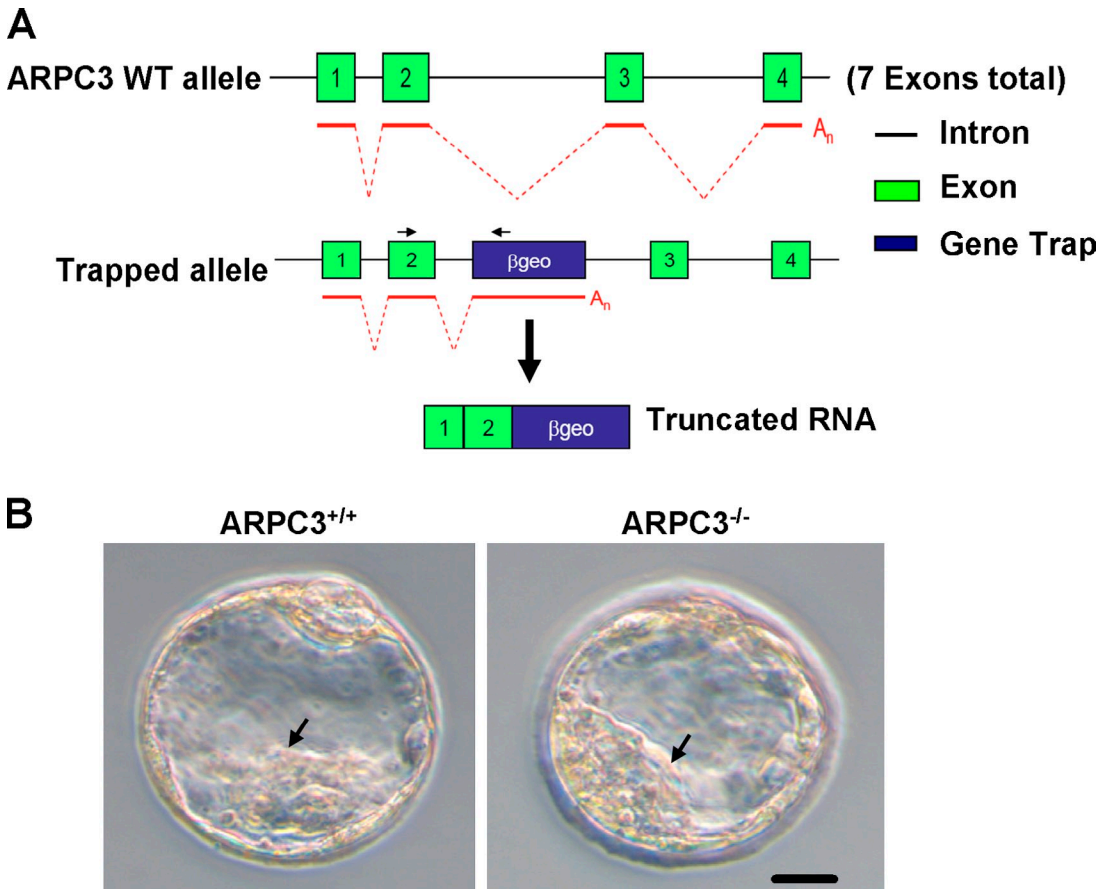

Figure S1. **Generation of ARPC3$^{+/-}$ gene-trap mouse and ARPC3$^{+/+}$ and ARPC3$^{-/-}$ ES cells.** (A) Schematic diagram describing ARPC3 wild-type (WT) and gene-trap alleles. (B) The morphology of ARPC3$^{+/+}$ and ARPC3$^{-/-}$ blastocysts showing healthy inner cell mass (arrows). Bar, 20 µm.

Published April 9, 2012

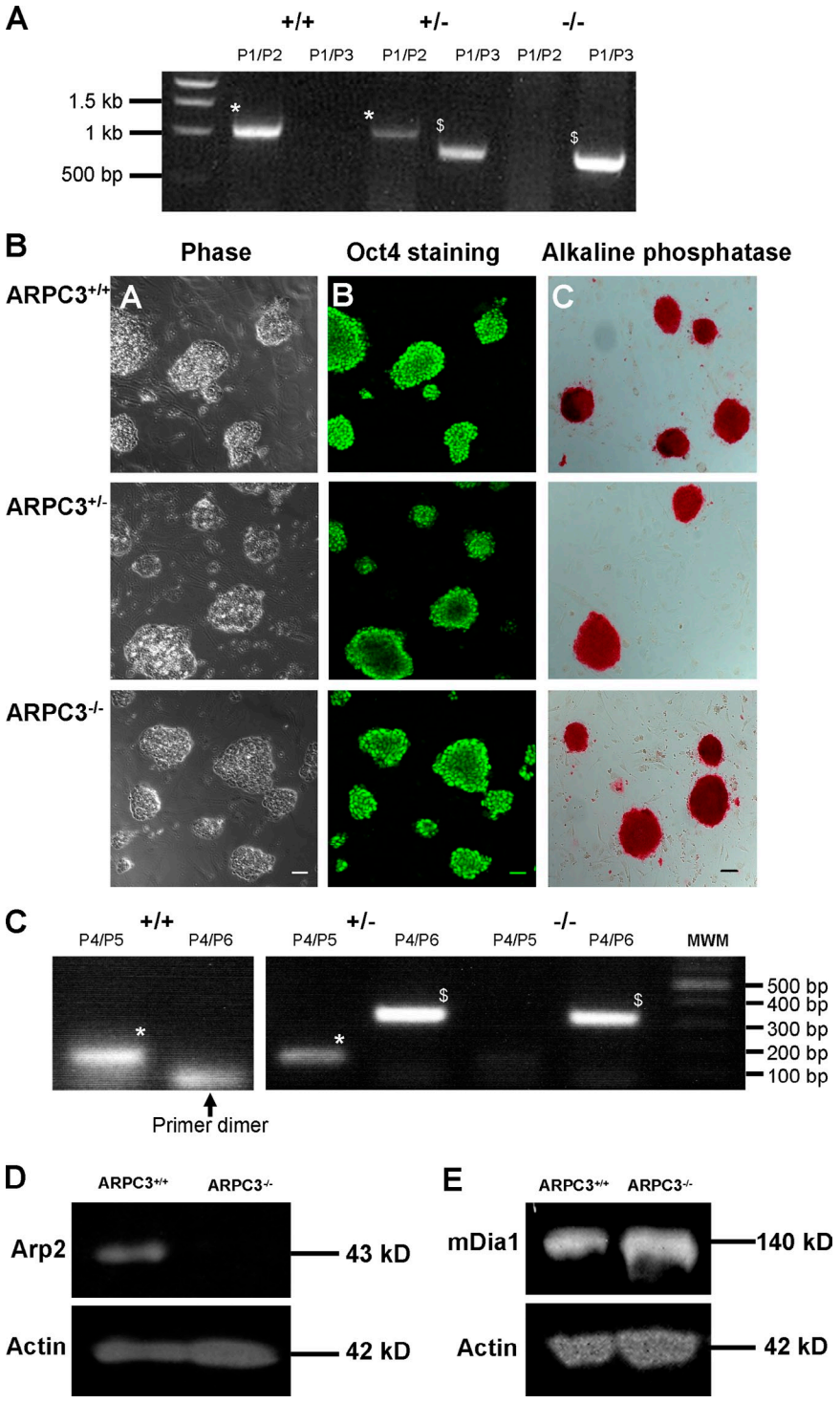

Figure S2. **Characterization of ARPC3$^{+/+}$ and ARPC3$^{-/-}$ ES cells.** (A) ARPC3$^{+/+}$ and ARPC3$^{-/-}$ ES cell genotyping. The wild-type allele was detected with a forward primer (P1) against a sequence in Exon2 with a reverse primer against an intronic region between Exon2 and 3 (P2), producing a PCR fragment of 1039 bp (*). For the mutant allele, the same forward primer as the above was used with a reverse primer against the βgeo region of the trapped trap cassette (P3), producing a fragment of 799 bp ($). (B) Analysis of ARPC3$^{+/+}$ and ARPC3$^{-/-}$ ES cell colonies with pluripotency markers. ES cell clones derived from ARPC3$^{+/+}$ and ARPC3$^{-/-}$ blastocysts were analyzed by immunofluorescence staining against Oct4 and processed for alkaline phosphatase activity (Thomson et al., 1998; Singh et al., 2008; J. Lee et al., 2010; Griffith et al., 2011). Bars: (left and middle panels) 50 µm; (right panels) 100 µm. (C) RT-PCR analysis of ARPC3$^{+/+}$, ARPC3$^{+/-}$ ES, and ARPC3$^{-/-}$ fibroblast cells confirm expected truncation of ARPC3 mRNA by gene-trap. The wild-type mRNA was detected with a forward primer designed on Exon2 (P4) and a reverse primer against a sequence in Exon4 (P5), producing an 181-bp fragment (*) by RT-PCR. The gene-trapped mRNA was detected with the same forward primer as the above and a reverse primer against a sequence in the βgeo region of the trap (P6), producing a 322-bp fragment ($) by RT-PCR. MWM: molecular weight marker. (D) Immunoblot analysis of total cell extracts using anti-Arp2 and anti-actin (Sigma-Aldrich) antibodies. Densitometry quantification after normalization to the actin band found that the Arp2 proteins in the ARPC3$^{+/+}$ cell was 8.6x that in ARPC3$^{-/-}$ cells. (E) Immunoblot analysis of total cell extracts using anti-mDia1 and anti-actin antibodies. Densitometry quantification after normalization to actin found that the mDia1 protein in ARPC3$^{+/+}$ cell was 0.91x that in ARPC3$^{-/-}$ cells.

Published April 9, 2012

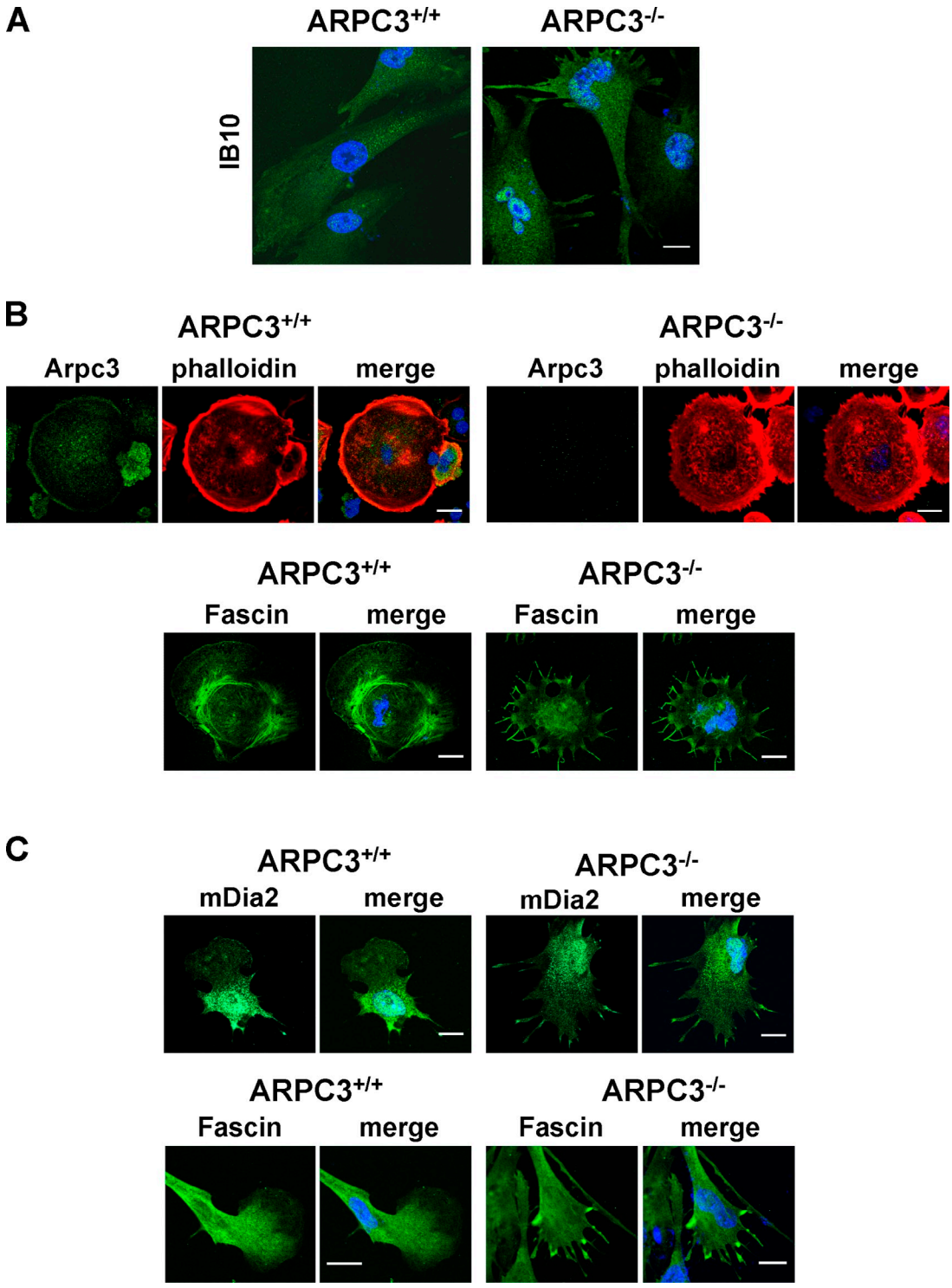

Figure S3. **Characterization of ARPC3$^{+/+}$ and ARPC3$^{-/-}$ fibroblast cells by immunofluorescence staining.** (A) Staining of the fibroblast marker IB10 (Pease et al., 1990; Rønnov-Jessen et al., 1992). (B) Staining of spreading cells with anti-ARPC3 and anti-fascin antibodies. We note that the latter antibody staining conditions are incompatible with phalloidin staining. (C) Staining of polarized cells with the anti-mDia2 and anti-fascin antibodies. The latter staining condition was also incompatible with phalloidin staining. Bars, 25 µm.

Published April 9, 2012

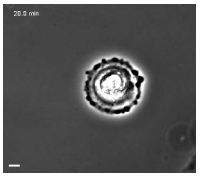

Video 1. **A spreading ARPC3$^{+/+}$ fibroblast cell.** ARPC3$^{+/+}$ fibroblast cells were trypsinized and allowed to reattach to fibronectin-coated surface. The time-lapse video shows the lamellipodia-based leading edge of spreading ARPC3$^{+/+}$ cells. The video was recorded for a period of 2 h with frames taken every 1 min on a microscope (Eclipse TE2000-E; Nikon). Bar, 25 µm.

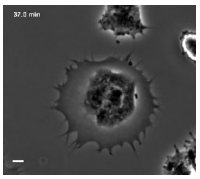

Video 2. **A spreading ARPC3 $^{-/-}$ fibroblast cell.** ARPC3$^{-/-}$ fibroblast cells were trypsinized and allowed to reattach to fibronectin-coated surface. The time-lapse video shows the FLP-dominated leading edge of spreading ARPC3$^{-/-}$ cells. The video was recorded for a period of 2 h with frames taken every 1 min on a microscope (Eclipse TE2000-E; Nikon). Bar, 25 µm.

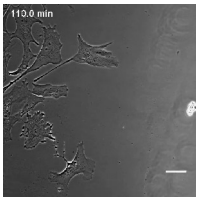

Video 3. **ARPC3$^{+/+}$ fibroblast cells migrating toward the wound.** ARPC3$^{+/+}$ fibroblast cells migrating toward the wound during a wound-healing assay were recorded every 5min for a period of 3.5 h using a microscope (LSM-510; Carl Zeiss). Bar, 50 µm.

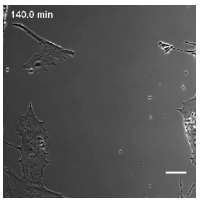

Video 4. **ARPC3$^{-/-}$ fibroblast cells migrating toward the wound.** ARPC3$^{-/-}$ fibroblast cells migrating toward the wound during a wound-healing assay were recorded every 5min for a period of 3.5 h using a microscope (LSM-510; Carl Zeiss). Bar, 50 µm.

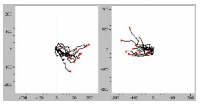

Video 5. **Trajectories of individual ARPC3$^{+/+}$ fibroblast cells during wound closure.** Single ARPC3$^{+/+}$ cells migrating at the wound edge were tracked using the ImageJ plug-in and trajectories during 10-h time-lapse recordings were plotted by bringing together the starting position of all cells. Trajectories represent the cells migrating from opposite sides of the wound edge. Dots represent the center of mass of individual cells.

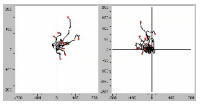

Video 6. **Trajectories of individual ARPC3$^{-/-}$ fibroblast cells.** Single ARPC3$^{-/-}$ cells migrating at the wound edge were tracked using the ImageJ plug-in and trajectories during 10-h time-lapse recordings were plotted by bringing together the starting position of all cells. Trajectories represent the cells migrating from opposite sides of the wound edge. Dots represent the center of mass of individual cells.

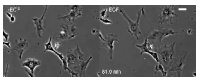

Video 7. **ARPC3$^{+/+}$ fibroblast cells responding to stimulation with 25 ng/ml EGF.** ARPC3$^{+/+}$ fibroblast cells on a fibronectin (5 µg/ml)-coated surface were recorded before and after stimulation with 25 ng/ml EGF. Notice the more vigorous lamellipodia activity after EGF addition. Phase-contrast movies were recorded using a microscope (Eclipse TE2000-E; Nikon) for 2 h with 1 min between frames. Bar, 50 µm.

Published April 9, 2012

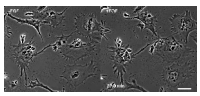

Video 8. **ARPC3$^{-/-}$ fibroblast cells responding to stimulation with 25 ng/ml EGF.** ARPC3$^{-/-}$ fibroblast cells on a fibronectin (5 µg/ml)-coated surface were recorded before and after stimulation with 25 ng/ml EGF. Notice the more vigorous lamellipodia activity after EGF addition. Phase-contrast movies were recorded using a microscope (Eclipse TE2000-E; Nikon) for 2 h with 1 min between frames. Bar, 50 µm.

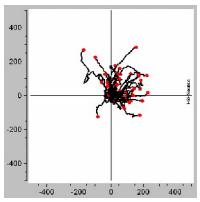

Video 9. **Trajectories of individual ARPC3$^{+/+}$ fibroblast cells migrating in the presence of an EGF gradient.** ARPC3$^{+/+}$ fibroblast cells were placed on a fibronectin (5 µg/ml)-coated µ-Slide and tracked for 12 h in the presence of an EGF gradient (500 ng/ml at source) on a microscope (Eclipse TE2000-E; Nikon). Trajectories of 43 individual cells from a single experiment were generated using the ImageJ plug-in from 12-h phase-contrast movies with frames 10 min apart. Dots represent the center of mass of individual cells.

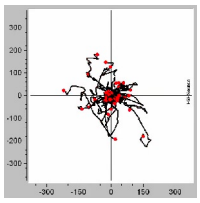

Video 10. **Trajectories of individual ARPC3$^{-/-}$ cells migrating in the presence of an EGF gradient.** ARPC3$^{-/-}$ fibroblast cells were placed on a fibronectin (5 µg/ml)-coated µ-Slide and tracked for 12 h in the presence of an EGF gradient (500 ng/ml at source) on a microscope (Eclipse TE2000-E; Nikon). Trajectories of 41 individual cells from a single experiment were generated using the ImageJ plug-in from 12-h phase-contrast movies with frames 10 min apart. Dots represent the center of mass of individual cells.

References

Griffith, G.J., M.C. Trask, J. Hiller, M. Walentuk, J.B. Pawlak, K.D. Tremblay, and J. Mager. 2011. Yin-yang1 is required in the mammalian oocyte for follicle expansion. *Biol. Reprod.* 84:654–663. http://dx.doi.org/10.1095/biolreprod.110.087213

Lee, J., J. Lee, E. Jung, Y.-S. Kim, K. Roh, K.-H. Jung, and D. Park. 2010. Ultraviolet A regulates adipogenic differentiation of human adipose tissue-derived mesenchymal stem cells via up-regulation of Kruppel-like factor 2. *J. Biol. Chem.* 285:32647–32656. http://dx.doi.org/10.1074/jbc.M110.135830

Pease, S., P. Braghetta, D. Gearing, D. Grail, and R.L. Williams. 1990. Isolation of embryonic stem (ES) cells in media supplemented with recombinant leukemia inhibitory factor (LIF). *Dev. Biol.* 141:344–352. http://dx.doi.org/10.1016/0012-1606(90)90390-5

Rønnov-Jessen, L., J.E. Celis, B. Van Deurs, and O.W. Petersen. 1992. A fibroblast-associated antigen: characterization in fibroblasts and immunoreactivity in smooth muscle differentiated stromal cells. *J. Histochem. Cytochem.* 40:475–486. http://dx.doi.org/10.1177/40.4.1552184

Singh, S.K., M.N. Kagalwala, J. Parker-Thornburg, H. Adams, and S. Majumder. 2008. REST maintains self-renewal and pluripotency of embryonic stem cells. *Nature*. 453:223–227. http://dx.doi.org/10.1038/nature06863

Thomson, J.A., J. Itskovitz-Eldor, S.S. Shapiro, M.A. Waknitz, J.J. Swiergiel, V.S. Marshall, and J.M. Jones. 1998. Embryonic stem cell lines derived from human blastocysts. *Science*. 282:1145–1147. http://dx.doi.org/10.1126/science.282.5391.1145

Published April 9, 2012

Table S1. **Leading edge protrusion and retraction rates and durations**

Rates / Genotype	Protrusion rate (μm/min)	Retraction rate (μm/min)	Protrusion duration (min)	Retraction duration (min)	Total # of kymographs
ARPC3$^{+/+}$	1.75 ± 0.05	2.18 ± 0.07	1.11 ± 0.03	0.86 ± 0.03	61
ARPC3$^{-/-}$	2.6 ± 0.07	2.74 ± 0.09	1.33 ± 0.02	1.29 ± 0.02	72
p-value	6.89E-37	1.00E-13	1.33E-9	1.12E-31	

Leading edge protrusion and retraction rates and durations were computed using the graphs generated from kymographs (see Fig. 3). Values are mean ± SEM. p-values were determined by the Student's *t*-test, and refer to the difference between the protrusion and retraction parameters comparing wild-type and mutant cells.

Published April 9, 2012

Table S2. **Quantification of leading edge dynamics**

Rates	Protrusion rate (μm/min)	Retraction rate (μm/min)	Protrusion duration (min)	Retraction duration (min)	Total # of kymographs
$ARPC3^{+/+}$ -EGF	1.43 ± 0.03	1.20 ± 0.03	1.06 ± 0.03	0.83 ± 0.02	65
$ARPC3^{+/+}$ +EGF	1.5 ± 0.02	1.33 ± 0.03	1.19 ± 0.04	0.82 ± 0.02	78
p-value	0.052	0.001	0.001	0.40	
$ARPC3^{-/-}$ -EGF	1.87 ± 0.04	1.82 ± 0.03	0.85 ± 0.02	0.78 ± 0.02	76
$ARPC3^{-/-}$ +EGF	2.17 ± 0.04	2.11 ± 0.03	0.93 ± 0.03	0.82 ± 0.02	70
p-value	5.80E-7	3.47E-6	0.009	0.05	

Quantification of leading edge dynamics by kymograph analysis of $ARPC3^{+/+}$ and $ARPC3^{-/-}$ fibroblast cells with or without stimulation with 25 ng/ml EGF. Values are mean ± SEM.